

Digital characterization of thrombolite-stromatolite reef distribution in a carbonate ramp system (terminal Proterozoic, Nama Group, Namibia)

Erwin W. Adams, John P. Grotzinger, Wesley A. Watters, Stefan Schröder, David S. McCormick, and Hisham A. Al-Siyabi

ABSTRACT

The stratigraphic architecture of a terminal Proterozoic carbonate ramp system (ca. 550 Ma, Nama Group, Namibia) was mapped quantitatively with digital surveying technologies. The carbonate ramp consists of a shoaling-upward ramp sequence in which thrombolite-stromatolite reefs developed at several stratigraphic levels. The reefs are associated with grainstone and heterolithic facies and exhibit diverse geometries and dimensions related to the position in the sequence-stratigraphic framework. Laterally extensive reefs with a tabular geometry developed when accommodation was relatively low, whereas discontinuous oblate dome-shaped reefs developed during times when accommodation space was relatively high. Collecting sedimentological and stratigraphic data digitally in an extensive canyon system allowed a comprehensive documentation of the three-dimensional (3-D) architecture and dimensions of the reefal buildups. Both deterministic and stochastic methods were used to extend outcrop observations to construct 3-D models that honor the observed stratigraphy. In particular, the accuracy with which dimensions of reefal buildups can be measured is critically important in the statistical modeling of the dome-shaped buildups. Calculations and corrections can be applied directly to the digital data set and serve as input during model building. The final 3-D model faithfully reproduces the outcrop distribution of facies and geological objects and has a high spatial resolution, compared

AUTHORS

ERWIN W. ADAMS ~ *Department of Earth, Atmospheric, and Planetary Sciences, Massachusetts Institute of Technology, 77 Massachusetts Avenue, Cambridge, Massachusetts 02139; present address: Shell International Exploration and Production B.V., Kessler Park 1, 2288 GS Rijswijk, Netherlands; erwin.adams@shell.com*

Erwin Adams received his M.Sc. degree (1996) and his Ph.D. (2001) in geology from the Vrije Universiteit Amsterdam, Netherlands. He worked for three years at the Massachusetts Institute of Technology (MIT), deploying digital methods for mapping and modeling reservoir-scale carbonate outcrops in the terminal Proterozoic of the Nama Group, Namibia, and the Devonian of the Canning basin, Western Australia. Erwin joined the Carbonate Team at Shell in 2004.

JOHN P. GROTZINGER ~ *Department of Earth, Atmospheric, and Planetary Sciences, Massachusetts Institute of Technology, 77 Massachusetts Avenue, Cambridge, Massachusetts 02139; grotz@mit.edu*

John Grotzinger is the Robert Shrock Professor of Geology at MIT. He received degrees in geology from Hobart College (B.Sc.), the University of Montana (M.Sc.), and Virginia Tech (Ph.D.). His research focuses on field-based outcrop studies of reservoir-scale heterogeneity, evaluation of biogeochemical events at the Precambrian–Cambrian boundary, and robotic investigations of the stratigraphic record of Mars.

WESLEY A. WATTERS ~ *Department of Earth, Atmospheric, and Planetary Sciences, Massachusetts Institute of Technology, 77 Massachusetts Avenue, Cambridge, Massachusetts 02139; watters@mit.edu*

Wesley A. Watters is a graduate student in geophysics at MIT. He studies the effects of large impacts on planetary evolution and is a member of the Mars Exploration Rover Athena Science Team. He also works on problems relating to the morphometry and morphogenesis of stromatolites and early skeletogenous metazoa.

STEFAN SCHRÖDER ~ *Department of Earth, Atmospheric, and Planetary Sciences, Massachusetts Institute of Technology, 77 Massachusetts Avenue, Cambridge, Massachusetts 02139; present address: Department of Geology, University of Johannesburg, Auckland Park 2006, P.O. Box 524, Johannesburg, Republic of South Africa; sts@rau.ac.za*

Stefan Schröder received geology degrees from the Universities of Würzburg, Germany (M.Sc.), and Bern, Switzerland (Ph.D.). Since then, he has

Copyright ©2005. The American Association of Petroleum Geologists. All rights reserved.

Manuscript received January 7, 2005; provisional acceptance March 16, 2005; revised manuscript received June 14, 2005; final acceptance June 16, 2005.

DOI:10.1306/061605050005

worked at MIT on Neoproterozoic reservoir rocks in Namibia and Oman. He is currently taking a post-doctoral study at the University of Johannesburg and studies Paleoproterozoic carbonates together with Nicolas Beukes. His research focuses on sedimentary processes and environmental factors governing sedimentation in the Precambrian.

DAVID S. MCCORMICK ~ *Schlumberger-Doll Research, 320 Bent Street, Cambridge, Massachusetts 02141; dmccormick@slb.com*

David McCormick is a senior research scientist and program manager at Schlumberger-Doll Research. He received geology degrees in sedimentology from Dartmouth College (B.A.), Columbia University (M.A.), and MIT (Ph.D.). Before Schlumberger, he worked at Chevron Petroleum Technology Company. His main interests lie in digital mapping and quantification of geology and outcrop analogs for reservoir characterization and modeling.

HISHAM A. AL-SIYABI ~ *Shell Exploration and Production Company, One Shell Square, P.O. Box 61933, New Orleans, Louisiana 70161; h.siyabi@shell.com*

Hisham A. Al-Siyabi holds an M.Sc. (1994) degree and a Ph.D. (1998) from the Colorado School of Mines. Hisham joined Petroleum Development Oman in 1999, and since 2001 has worked as a geologist and seismic interpreter on the South Oman Exploration Team, working exclusively on the terminal Proterozoic intrasalt Ara stringers. In 2005, Hisham joined Shell Exploration and Production Company as an exploration geologist.

ACKNOWLEDGEMENTS

We are grateful to Marianne and Rob Field for their hospitality and access to the Zebra River farm. We express many thanks to the digital geology mapping crew of Zebra River: Abdullah Al-Habsy, Rashid Al-Hashimi, Rashid Al-Hinai, Omar Al-Ja'aidi, Issa Al-Mazroui, Hamad Al-Shuaily, Aus Al-Tawil (including photography), Joachim Amthor, Tony Dickson (including photography), Leon Hoffmann, Marc Newell, Mia van Steenwinkel (including photography), and Rachel Wood (including photography). Logistical support was provided by the Geological Survey of Namibia. We also thank Wim Dewulf for logistical support. Support for this project was provided by National Science Foundation Grants EAR-9904298 and EAR-0001018, Schlumberger Oilfield Research, and Petroleum Development Oman. Reviews from Paul M. Harris, William C. Parcell, and Peter D. Warwick helped to improve this article.

with petroleum industry reservoir models. The organization of the reefal buildups in the stratigraphic framework has direct implications for reservoir continuity and connectivity in analogous settings. The digital characterization and 3-D outcrop models presented in this article can be subsequently used to condition dynamic reservoir-simulation modeling of geologically similar areas.

INTRODUCTION

To better understand the spatial heterogeneity in the properties that determine fluid flow performance of petroleum and groundwater reservoirs, it is instructive to create three-dimensional (3-D) geologic models and to use these static models as input for dynamic reservoir modeling (Weber, 1986; Kerans and Tinker, 1997; Grötsch and Mercadier, 1999; Lucia, 1999; Grötsch et al., 2003; Larue and Legarre, 2004). Outcrop models are of particular interest because they include observations on many scales and in 3-D (White and Barton, 1999; Willis and White, 2000; Li and White, 2003). However, it is commonly difficult or impossible to obtain 3-D quantitative data from mountain-size outcrops. Carbonate ramps are a good example. They have received a great deal of attention in the last decade, and much is known about their tectonic setting, sequence-stratigraphic development, hydrodynamics, and sedimentary facies organization (Burchette and Wright, 1992; Tucker et al., 1993; Wright and Burchette, 1998). However, with widths of approximately 50–200 km (31–124 mi), lengths of easily more than 200 km (124 mi), but a thickness of a few hundreds of meters, carbonate ramps commonly are too extensive and relatively thin for quantitative geometric analyses (Burchette and Wright, 1992). However, geologic outcrop studies can drastically be improved using digital data acquisition methods such as differential global positioning systems or terrestrial scanning lidar to map quantitatively large-scale outcrops (e.g., Adams et al., 2004; Verwer et al., 2004; Bellian et al., 2005). Two of the advantages to digital data collection (Kramer, 1998; Thurmond et al., 1999; Wolf, 2002) are the ability to rapidly visualize and analyze digital data in 3-D in the field. In addition, the collected spatial coordinates can be tagged with additional geologic information (e.g., lithology or sedimentary facies, fossil type, stratigraphic-surface type, etc.), which facilitates building 3-D data sets with geological significance. For geologists who work with subsurface data and want to hierarchically model geological bodies in large-scale reservoir models (Dreyer et al., 1993; Geehan and Underwood, 1993; White and Willis, 2000), digital data collection allows one to quantify accurately and rapidly length scales of, for example, sedimentary bodies. Furthermore, quantitative digital data sets can be directly used to construct static models, which, in their turn, can serve as input in dynamic reservoir-simulation models.

In this article, we used high-resolution outcrop data collected with digital surveying tools from terminal Proterozoic ramp

carbonates of the Nama Group of Namibia to create 3-D outcrop models. These outcrops provide excellent analogs for hydrocarbon reservoirs in the subsurface of Oman (Grotzinger and Amthor, 2002). First, we sketch out the sedimentology and sequence stratigraphy of the carbonate ramp. Second, we report on deterministic as well as stochastic modeling techniques used to create 3-D stratigraphic models. Finally, we discuss implications of the model and particularly of the influence of the organization and geometrical diversity of reefal buildups in carbonate ramp systems.

GEOLOGIC BACKGROUND

Carbonate and siliciclastic sediments of the terminal Proterozoic to Cambrian Nama Group of southern Namibia were deposited in shallow-marine and fluvial depositional environments in a foreland basin setting (Germs, 1983; Gresse and Germs, 1993; Saylor et al., 1995). The foreland basin in which the Nama Group was deposited developed because of convergence along the western and northern margins of the Kalahari craton and overthrusting in the Gariep and Damara orogens (Figure 1) (Miller, 1983; Stanistreet et al., 1991; Germs, 1995). The Nama foreland basin is subdivided

into a northern and southern subbasin (Germs, 1974; Saylor et al., 1998). In the northern Zaris subbasin, the basal Kuibis Subgroup of the Nama Group forms a well-developed, storm- and wave-dominated carbonate ramp (Figure 2A) (Saylor et al., 1998; Smith, 1998; Grotzinger, 2000). The Kuibis Subgroup is subdivided into four members (Figure 2B) (Germs, 1983) that record the overall increase in accommodation space as the basin subsided in front of the cratonward-advancing orogenic wedge (Grotzinger, 2000). A transgressive tidal sandstone, the Kanies Member, makes up the basal unit and represents initial flooding over crystalline basement (Germs, 1983; Saylor et al., 1998; Grotzinger, 2000). The Omkyk Member represents shallow-water ramp carbonates; the Hoogland Member contains deeper water carbonate ramp facies (Smith, 1998; Grotzinger, 2000). Basinal shale is represented by the Urikos Member (Germs, 1983). Geochronologic constraints for the Kuibis Subgroup in the Zaris subbasin (Figure 2B) are provided by a volcanic ash bed that yields a U-Pb zircon age of 548.8 ± 1 Ma (Grotzinger et al., 1995), carbon isotope stratigraphy (Smith, 1998; Grotzinger, 2000), and the distributions of Ediacaran, *Cloudina*, and *Namacalathus* fossils (Grotzinger et al., 1995, 2000; Watters and Grotzinger, 2001).

The carbonate ramp of the Kuibis Subgroup (Figure 2A) is exceptionally well exposed in the Zaris

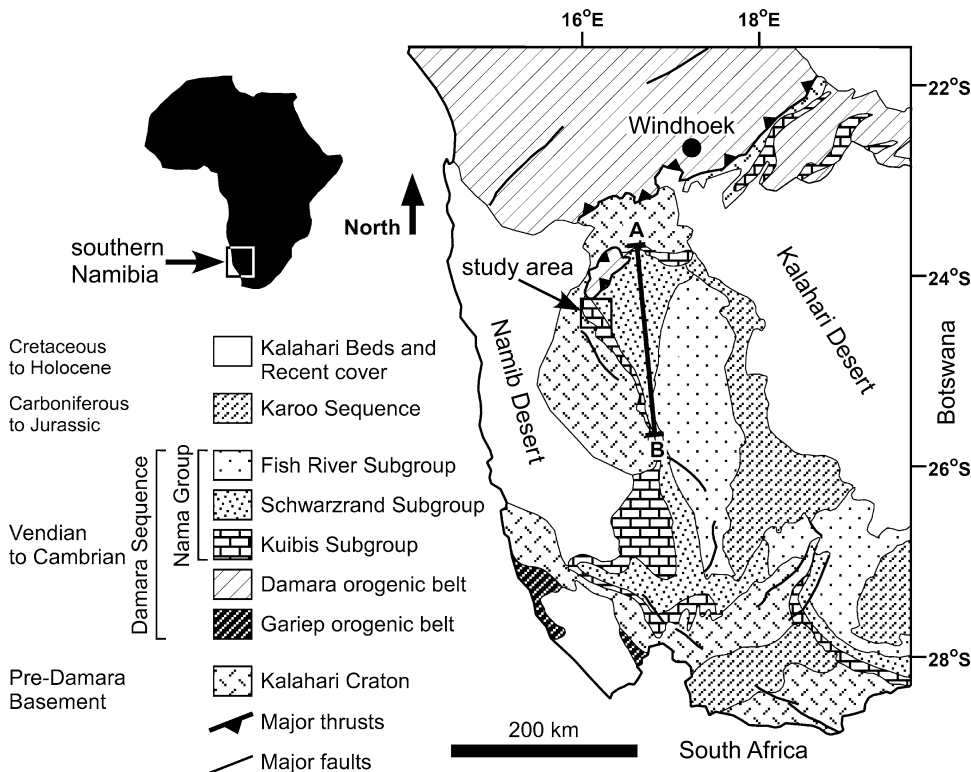
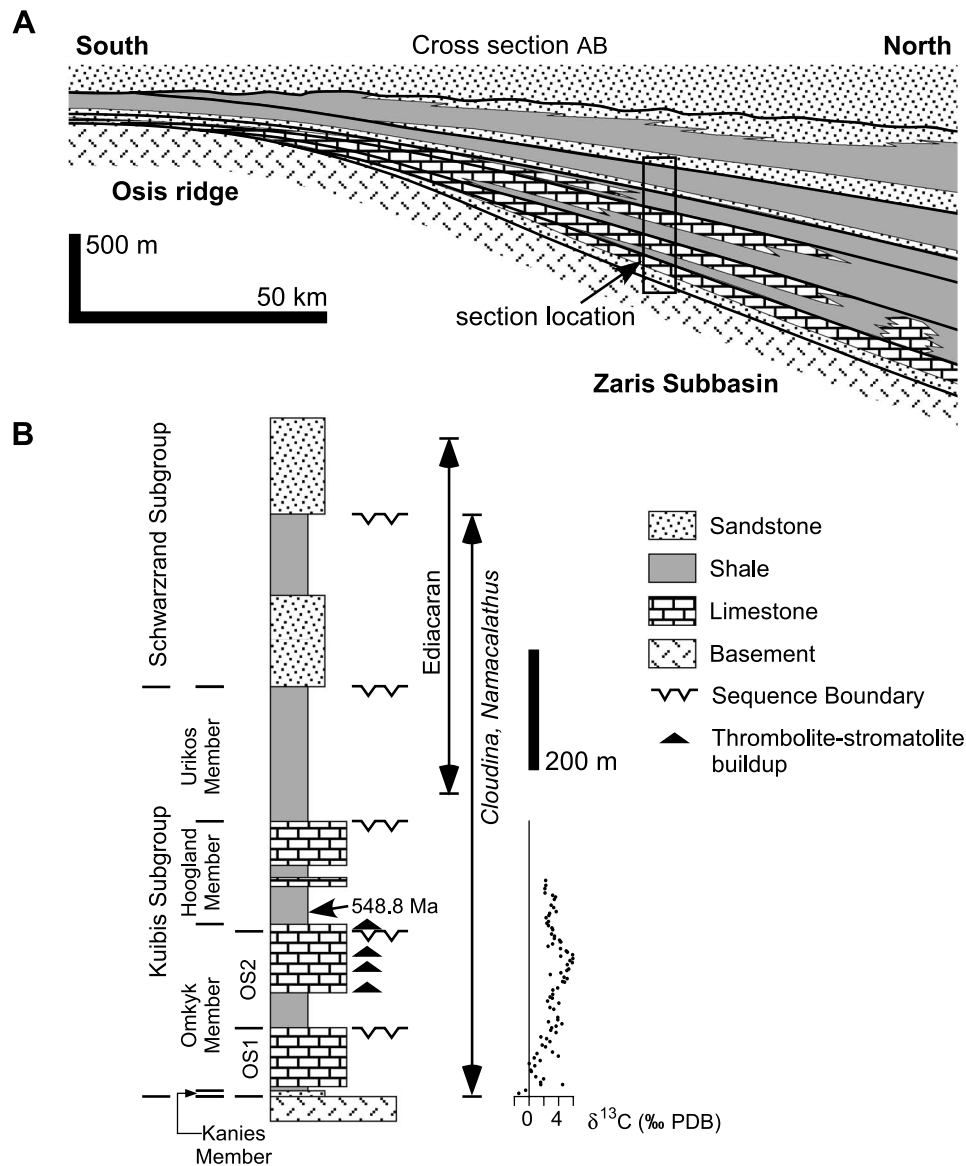


Figure 1. Geologic map of southern Namibia showing major sequences including the regionally widespread Nama Group. The analyzed carbonate ramp belongs to the Kuibis Subgroup of the Nama Group (see arrow and box locating the study area). The black line indicates north to south cross section AB through the Zaris subbasin shown in Figure 2A. Modified from Adams et al. (2004).

Figure 2. Geologic and stratigraphic setting of the lower Nama Group. Modified from Adams et al. (2004). (A) North to south cross section AB (for the location, see Figure 1) through the Zaris subbasin showing the carbonate ramp of the Kuibis Subgroup. From the Osis Ridge northward, the carbonate ramp thickens, and facies change to deeper water depositional systems. The box and arrow approximate the location and setting of the area of study. Modified from Germs (1983). (B) Generalized stratigraphy of the Kuibis Subgroup and the overlying Schwarzsrand Subgroup (for the location, see A). Omkyk sequence 2 (OS2) has several stratigraphic levels in which thrombolite-stromatolite buildups are found. An ash bed in the middle Kuibis Subgroup yielded an age of 548.8 ± 1 Ma (Grotzinger et al., 1995). Sequence-stratigraphic and isotope data from Smith (1998); biostratigraphic data from Grotzinger et al. (1995, 2000).



Mountains where a canyon system provides 3-D exposures (Figure 3). Shallow-water ramp carbonates, i.e., the Omkyk Member of the Kuibis Subgroup, are well exposed on the Zebra River and Donkergange farms, where they have a stratigraphic thickness of approximately 225 m (738 ft), paleogeographically dip toward the northwest, and structurally dip $2\text{--}5^\circ$ toward the northeast (Figure 3A). The Omkyk Member contains two coarsening-upward shoaling sequences; however, lithostratigraphic boundaries do not exactly match sequence-stratigraphic boundaries (Figure 2B) (Saylor et al., 1995, 1998; Smith, 1998; Grotzinger, 2000). The first sequence, Omkyk sequence 1 (OS1), is represented mostly by shelf grainstones. Omkyk sequence 2 (OS2) contains, besides abundant grain-

stones, thrombolite-stromatolite reefs that developed at several stratigraphic levels (Figure 2B) (Grotzinger, 2000).

SEDIMENTOLOGY AND FACIES

Sedimentary facies of the Omkyk Member of the Kuibis Subgroup clearly show evidence of deposition on a storm- and wave-dominated carbonate ramp (Grotzinger, 2000). The sedimentary facies of the carbonate ramp can be subdivided into inner-, mid-, and outer-ramp settings (cf. Burchette and Wright, 1992): the inner ramp formed above fair-weather wave base and was constantly agitated by waves; the midramp was

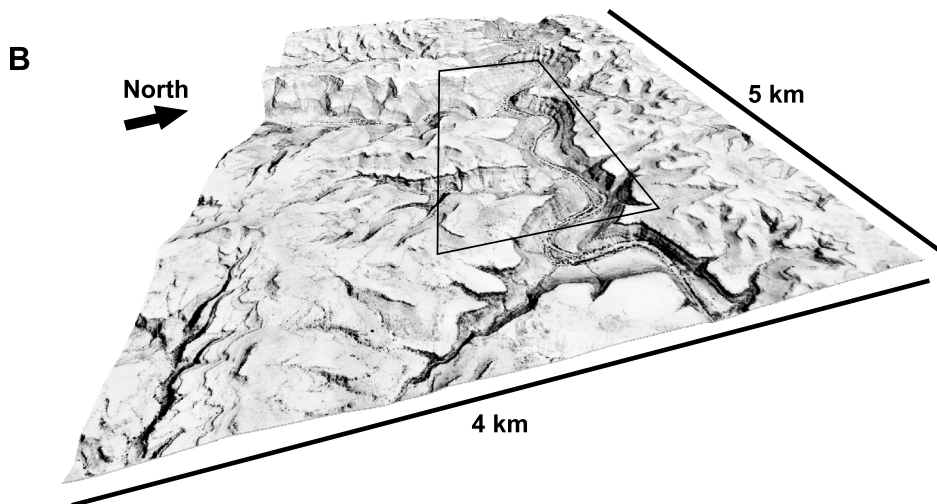
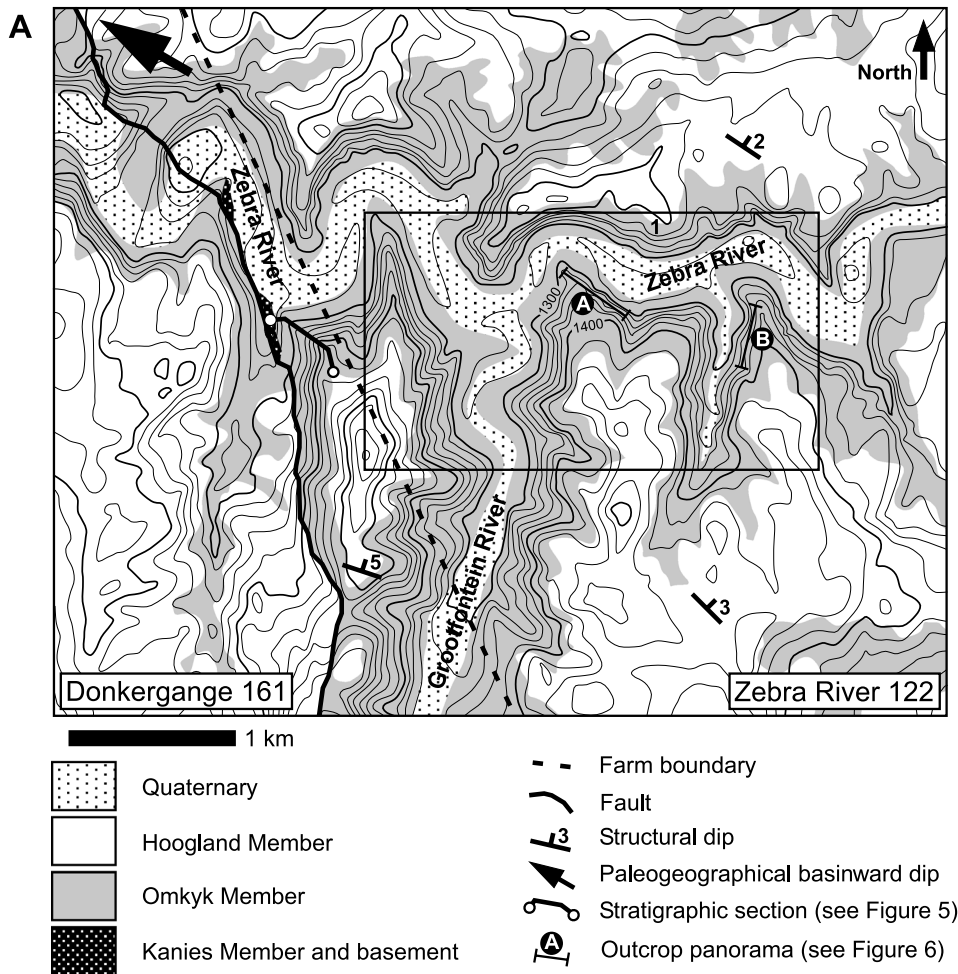


Figure 3. Setting of the study area illustrating a canyon system. (A) Geologic map of the Zebra River and the Donkergange farms (see names with numbers in boxes). Excellent 3-D exposures of the Omkyk Member are found along the Zebra and Grootfontein rivers. Note the locations of the outcrop panorama (see Figure 6) and stratigraphic section (see Figure 5). The box locates the 3-D outcrop model presented in this article. (B) Digital elevation model (DEM) with the superimposed aerial orthophotograph of the study area looking in a paleogeographically down-dip direction. Horizontal grid size of DEM is 10×10 m (33×33 ft); orthophotograph has 1×1 -m (3.3×3.3 -ft) pixel size. Individual trees can be seen in the river bed. The same area is covered as the map in (A) (for comparison, also see boxes).

frequently influenced by waves and storms; the outer ramp was infrequently reworked by storms. The basin contains deposits formed solely below storm-wave base, but may include storm-triggered turbidite deposits (Grotzinger, 2002). In what follows, we describe the facies in the order of increasing water depth.

Sandstone Facies

The sandstone facies consists of well-sorted, fine- to coarse-grained sandstones with lenticular and flaser bedding forming decimeter-thick beds. Mudstone rip-up clasts are commonly present at the base of sandstone

beds. The sandstones are interbedded with siliciclastic mudstones and siltstones as well as coarse-grained quartzites. Centimeter-scale unidirectional cross-bedding containing mud drapes, hummocky cross-stratification, and symmetrical ripples are also characteristic of this facies. Deposition of the sandstone facies is interpreted to have occurred in a tidal- to shallow-marine environment in an inner-ramp setting.

Grainstone Facies

The grainstone facies is typified by coarse-grained grainstones and fine- to medium-grained grainstones. Sedimentary structures in both types include planar, swaley, hummocky, wavy, and trough cross-stratification (Grotzinger, 2002). Grainstones are composed of millimeter-scale intraclasts, coated grains, peloids, and *Cloudina* fragments (Grotzinger, 2002).

The coarse-grained grainstones form meter-scale amalgamated beds with abundant large-scale hummocky and trough cross-stratification (Figure 4A). Deposition is interpreted to have occurred in shoals and bars that were located on the upper reaches of a high-energy shoreface strongly influenced by waves and currents in an inner-ramp setting.

The fine- to medium-grained grainstones form decimeter-scale beds and are interbedded with mudstones, siliciclastic shale, and irregular laminite; rip-up clasts and deformation structures are commonly present (Figure 4B). They are interpreted to have been deposited under moderately energetic conditions, with occasional periods of quiescence. Deposition occurred behind grainstone shoals and bars in an inner-ramp setting.

Thrombolite-Stromatolite Reef Facies

The reefs are composed of stacked columns separated by intercolumn fills. Columns contain both stromatolitic (laminated) and thrombotic (clotted) internal textures (Kennard and James, 1986). Columns are well developed and reach heights of up to several meters (Figure 4C). In plan view, columns are round to highly elliptical, with decimeter-scale short axes and meter-scale long axes. In general, the cores of columns are thrombotic, becoming stromatolitic toward the margin (Figure 4D). The columns have a consistent elongation with an azimuth of 270–310° perpendicular to the inferred strike of the Omkyk ramp (Grotzinger, 2000). Centimeter- to decimeter-wide intercolumn fills consist of trough cross-bedded, fossiliferous packstone-grainstone and mudstone.

The consistent column elongation and trough cross-bedded intercolumn fills indicate high-energy conditions in the thrombolite-stromatolite reef facies. Growth of reefs occurred in an inner-ramp setting.

Intraclast Breccia Facies

The intraclast breccia facies consists of jumbled intraclasts in a fine-grained matrix forming decimeter- to meter-scale beds (Figure 4E). Clasts are poorly sorted and angular. Beds show no grading and allochthonous sediments are absent. The intraclast breccias are associated with storm-generated, hummocky cross-stratified grainstones. Deposition is interpreted to have occurred in a storm-dominated environment in a mid-ramp setting (for a discussion and overview of these type of deposits, see Pratt, 2002).

Irregular Laminite Facies

This facies consists of very thin to thinly bedded irregular laminite interbedded with thin-bedded mudstones, fine-grained grainstones, and intraclast breccias (Figure 4F). Facies are associated in meter-scale shoaling cycles with shale-rich bases and grainstone caps (Grotzinger, 2002). Decimeter-scale thrombolite columns developed locally. Deposition is interpreted to have occurred in the shallowest setting of the mid-ramp, forming close to fair-weather wave base.

Heterolithic Facies

The heterolithic facies contains mostly siliciclastic shale (up to 50%) interbedded with thinly bedded mudstones, irregular laminites, and thinly bedded, fine-grained grainstones. Grainstones exhibit planar stratification, quasiplanar stratification, and small-scale hummocky cross-stratification. Deposition is interpreted to occur in an outer-ramp setting near the limit of the storm wave base.

STRATIGRAPHIC ARCHITECTURE

Ramp carbonates of the Omkyk Member form two coarsening-upward shoaling sequences (OS1 and OS2; Figure 2B). A measured stratigraphic column provides a detailed stratigraphic framework for both sequences (Figure 5). Only OS2 was digitally mapped because it contains several intervals in which thrombolite-stromatolite reefs developed. OS2 was subdivided

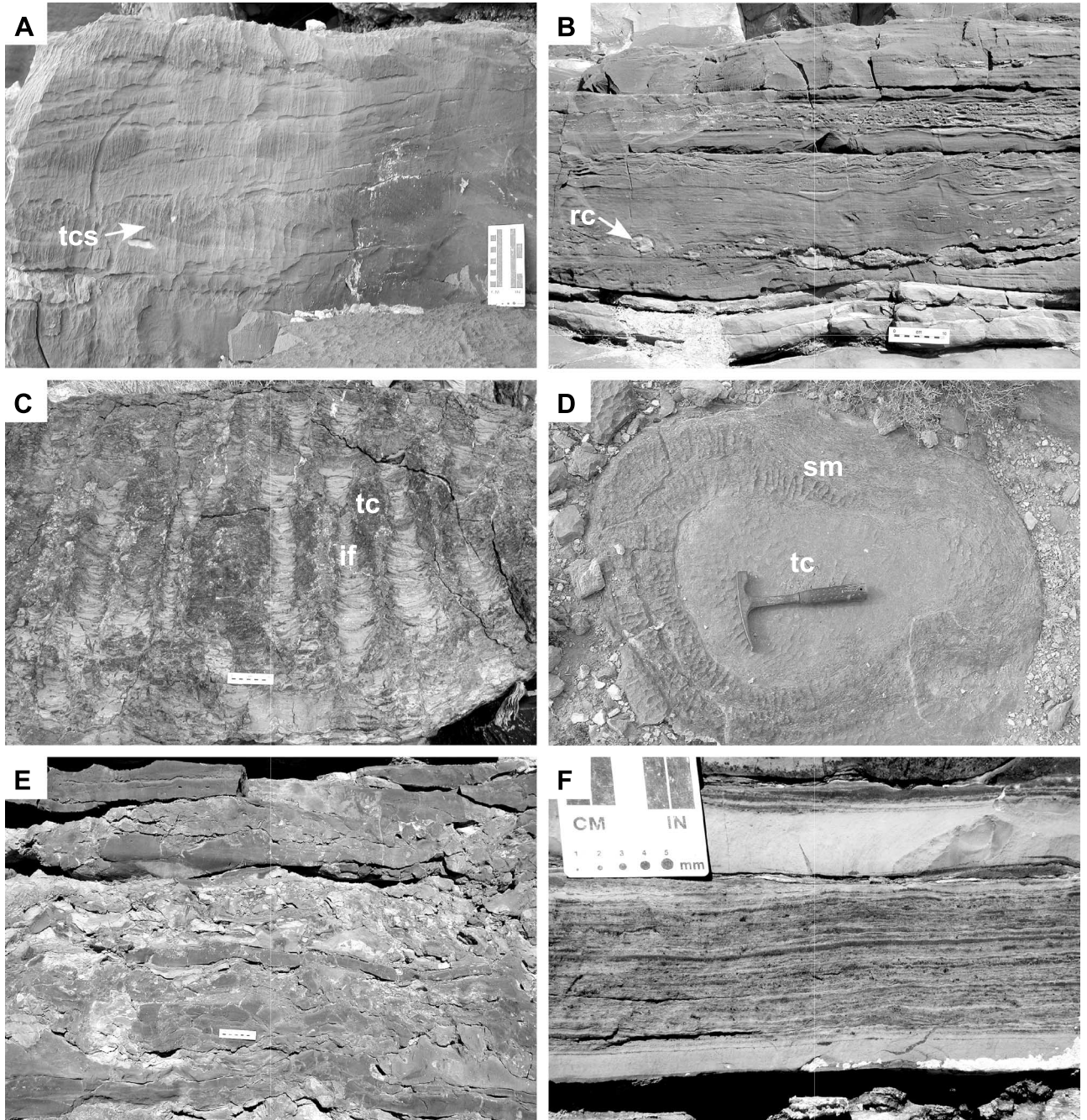
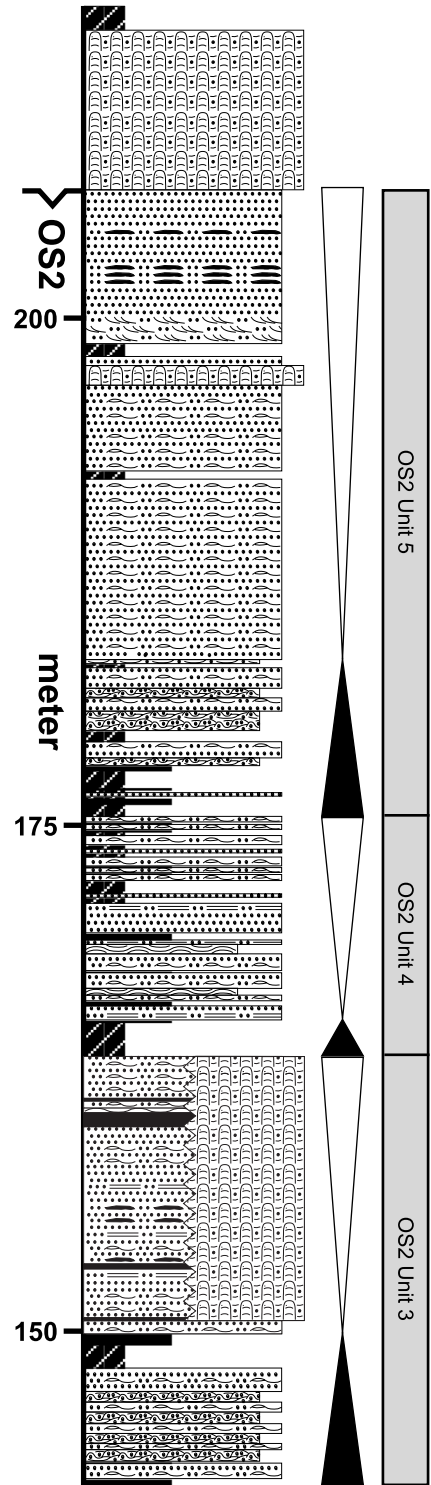
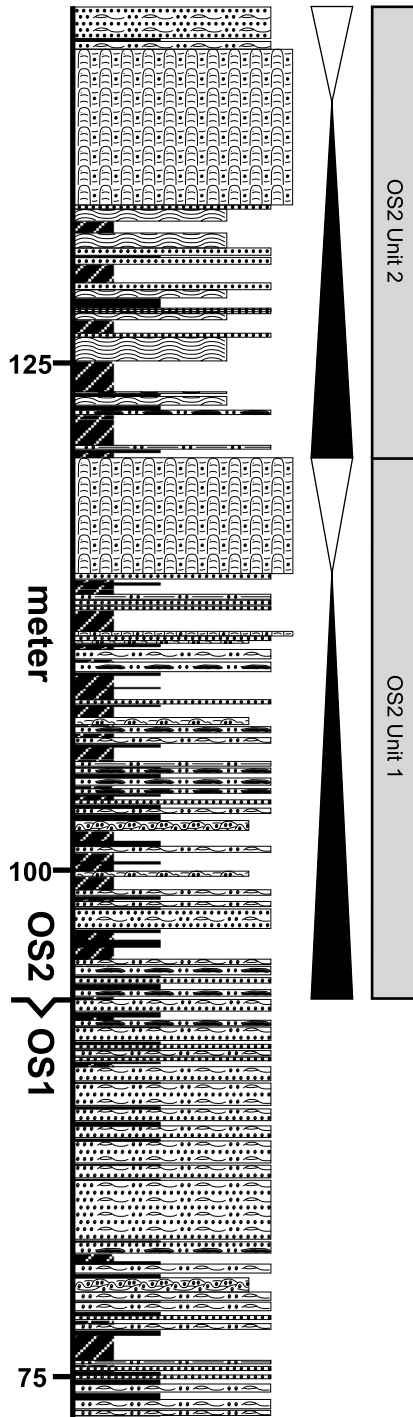
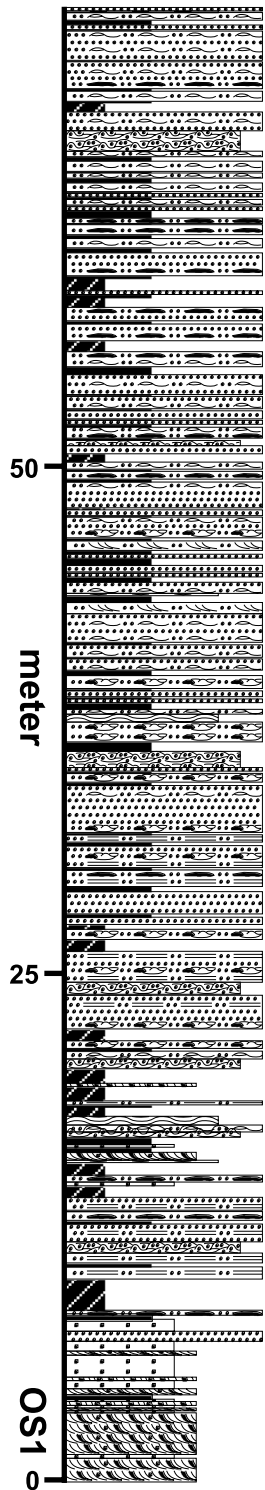

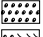

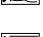














Figure 4. Representative photographs of sedimentary facies. (A) Amalgamated beds of coarse-grained grainstones with large-scale hummocky and trough cross-stratification (tcs). Scale bar is 10 cm (4 in.). (B) Fine- to medium-grained grainstone with swaley cross-stratification and centimeter-scale rip-up clasts (rc). Scale bar is 10 cm (4 in.). (C) Well-developed columns with thrombolitic texture (tc). Individual columns reach heights of up to 1 m (3.3 ft). Intercolumn fills (if) contain interbedded mudstone and fossil-rich packstones and grainstones. Scale is approximately 12 cm (4.7 in.) long. (D) Thrombolite-stromatolite column in plan view with thrombolitic texture (tc) in the center of the column and stromatolitic texture at the margin (sm). Hammer is 30 cm (12 in.) long. (E) Intraclast breccia with jumbled intraclast in a muddy to fine-grained matrix. White piece of paper is approximately 12 cm (4.7 in.) long. (F) Irregular laminite with mudstone beds at base and top. Note the millimeter-scale crinkly laminae. Thin dark layers are fine-grained grainstones.



-  thrombolite-stromatolite reef
-  grainstone with massive bedding
-  grainstone with through cross-bedding
-  grainstone with hummocky cross-stratification
-  grainstone with planar bedding
-  grainstone with rip-up clasts
-  grainstone with deformation structures

-  intraclast breccia
-  sandstone with trough cross, lenticular, and flaser bedding
-  siliciclastic siltstone
-  irregular laminite
-  siliciclastic shale or lime mudstone
-  covered interval

-  unit transgressive systems tract
-  unit highstand systems tract
-  sequence boundary (see Figure 2)

into five mappable sequence-stratigraphic units of roughly the same order and thickness of 15–25 m (49–82 ft) (OS2 units 1–5; Figures 5–7). For these five units of OS2, intervals can be recognized, which are dominated by either (1) heterolithic facies, including siliciclastic shale, lime mudstone, irregular laminite, intraclast breccia, and thin layers of fine-grained grainstone; (2) grainstone facies containing mostly coarse-grained grainstones and fine- to medium-grained grainstones; or (3) thrombolite-stromatolite reef facies (Figures 5–7). Within the canyon system, the grainstone- and heterolithic-dominated intervals tend to be uniform in thickness and laterally extensive. In cross section, the reefal buildups have morphologies ranging from tabular to oblate dome shaped and are laterally extensive or discontinuous (Figures 6, 7). During the development of thrombolite-stromatolite reefs, the synoptic relief was on the order of a few meters, and heterolithic or grainstone facies were deposited concurrently. Therefore, in this article, when we refer to a reefal buildup with either a tabular or dome-shaped morphology, we describe the overall present-day geometry as observed in outcrop in cross section and do not invoke depositional geometries. We did not investigate the internal geometry of the reefal buildups.

Sequence-Stratigraphic Development of Reefal Buildups

The first unit of OS2 contains abundant heterolithic facies; thrombolite-stromatolite reefs developed during the final stage of this unit (Figures 5, 7). However, outcrop conditions limited the documentation of geometries and distribution of these thrombolite-stromatolite reefs. Outcrops along the updip section only partially expose unit 1.

The next two units both contain reefal buildups; however, the geometries and facies association of the reefs differ substantially. Buildups of unit 2 are discontinuous, with oblate dome-shaped morphology; unit 3 buildups exhibit geometries that have a tabular morphology and are laterally extensive (Figure 7).

The lower part of unit 2 is dominated by heterolithic and irregular laminite facies (Figure 5). The

onset of reef growth is interpreted to have occurred during a transgressive systems tract when the reef was associated with heterolithic facies (Figure 8A). During the first stage of reef growth, the buildups only aggraded (Figure 8A, B). Later, the reefs started to prograde and became more and more associated with grainstone facies (Figures 7, 8A). This stage is interpreted as the highstand systems tract of unit 2. When accommodation space decreased even further, grainstone deposition covered the thrombolite-stromatolite reefs completely (Figures 6–8A), which implies that the increased sediment flux of clastic carbonates (i.e., grainstones) on the ramp terminated reef growth. The observed morphology of the buildups is oblate dome shaped in cross section and circular in plan view (i.e., horizontal cross section); the synoptic relief was on the order of a couple of meters. The development of thrombolite-stromatolite reefs as discontinuous dome-shaped buildups is interpreted to occur during times of high accommodation and reduced sediment input (Burchette and Wright, 1992; James and Bourque, 1992; Grotzinger, 2000).

The lower part of unit 3 is arranged in meter-scale parasequences that are composed of intraclast breccias grading into hummocky cross-stratified grainstones (Figure 5). Parasequences several meters thick each of amalgamated hummocky cross-stratified grainstones with heterolithic facies at their bases dominate the upper part of unit 3 and form a laterally continuous sheetlike belt (Figures 5–7). A laterally extensive, thrombolite-stromatolite reef with tabular morphology interfingers with this grainstone-dominated interval (Figures 7, 8C). The synoptic relief of the reef with respect to the grainstone beds is not high and roughly up to 1 m (3.3 ft). The interfingering illustrates a contemporaneous association with grainstone facies, and therefore, the reef is interpreted to have formed during a time when accommodation and water depths were relatively low, i.e., the highstand systems tract of unit 3 (Figure 5). Consequently, a laterally extensive tabular morphology developed.

The top of the last two units, units 4 and 5, are both dominated by grainstone facies (Figures 5, 7).

Figure 5. Detailed stratigraphic column and sequence-stratigraphic interpretation of OS2 (see Figure 3 for location of section in study area). In the field, five mappable units of roughly the same order were recognized for OS2. For the upper part of unit 3, the measured section crossed an interval dominated with grainstone facies. In other parts of the canyon, a thrombolite-stromatolite reef is found at this stratigraphic level and laterally interfingers with these grainstones. This is schematically illustrated by the zigzag pattern. A laterally continuous thrombolite-stromatolite reef is capping OS2 (cf. Grotzinger, 2000).

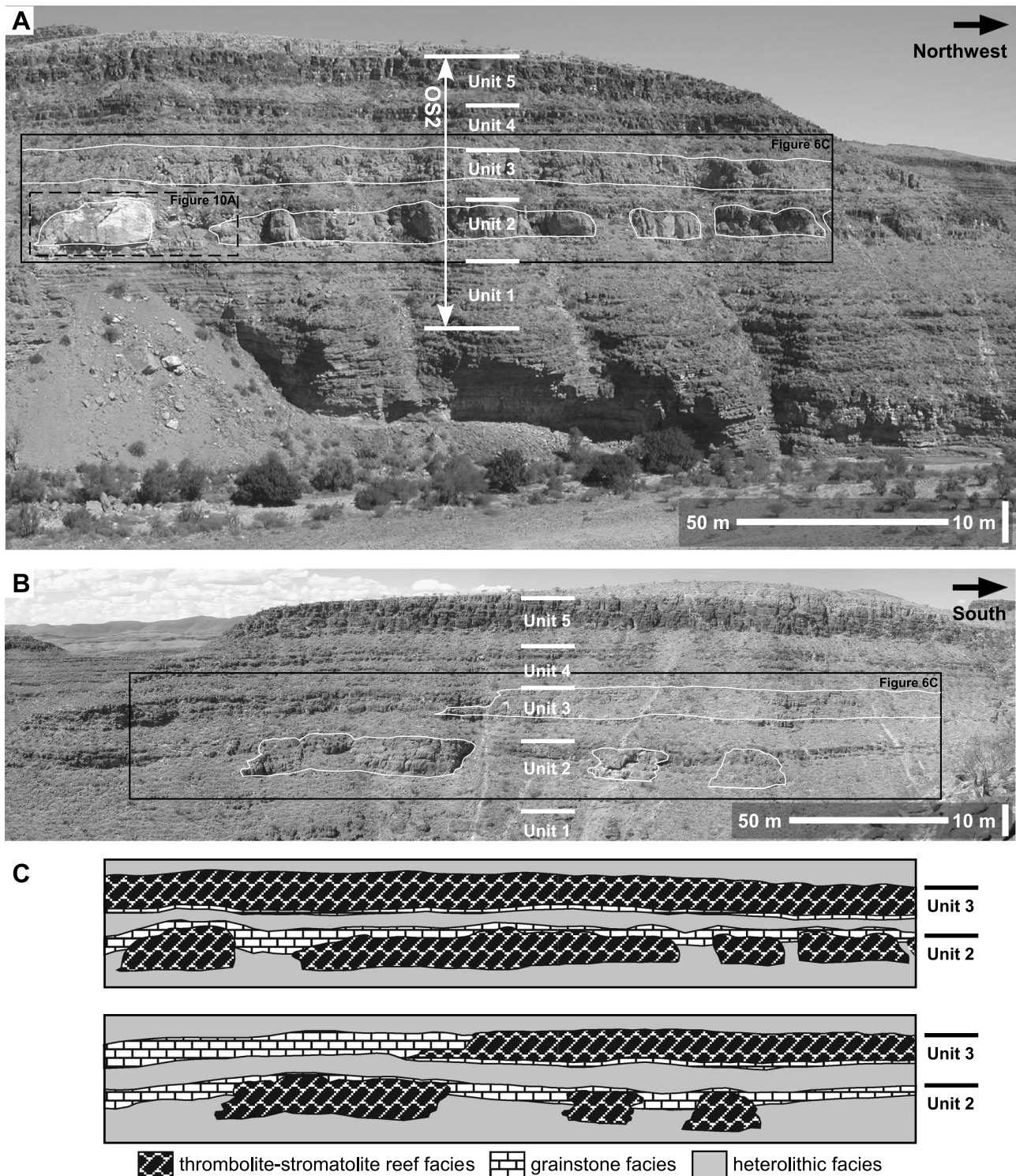


Figure 6. (A) Panoramic photograph of the outcrop (for the location, see Figure 3A) showing the coarsening-upward shoaling sequence of OS2 subdivided into five mappable units. Intervals can be recognized, which are dominated by heterolithic-, grainstone-, or thrombolite-stromatolite reef facies. Thrombolite-stromatolite reefs are found at several stratigraphic levels. Intervals dominated by grainstone facies (dark and well-bedded rocks) commonly form extensive sheets. Both thrombolite-stromatolite reefs and grainstones are interbedded with intervals dominated by heterolithic facies. (B) Panoramic photograph of outcrop (for the location, see Figure 3A) illustrating the lateral variation in reef geometry and continuity. The reef of unit 3 laterally interfingers with a grainstone facies-dominated interval. (C) Line drawings of outcrop panorama (see boxes in A and B for location) illustrating the architecture and dominant facies present in units 2 and 3.

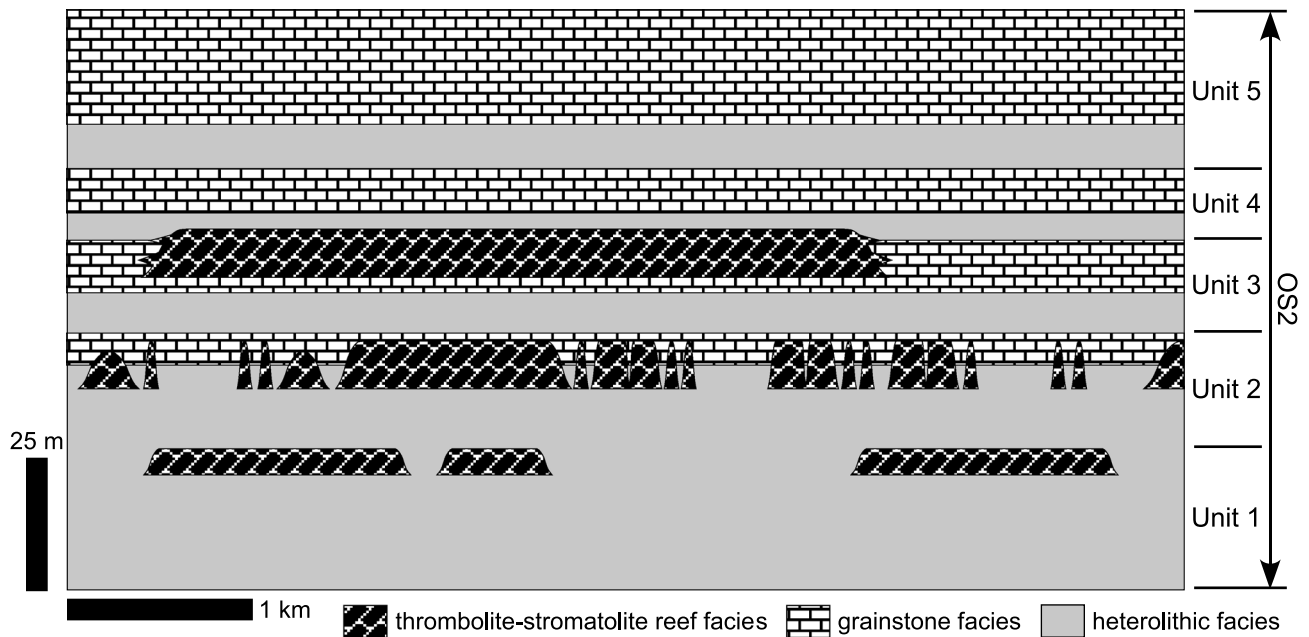


Figure 7. A schematic sketch of the stratigraphic architecture of Omkyk sequence 2. The coarsening-upward shoaling sequence is recognized by an increase in grainstone-dominated intervals; thrombolite-stromatolite reefs and heterolithic facies decrease toward the top of the sequence. Reefal buildups display a wide variety of geometries and dimensions. The sequence-stratigraphic position at the onset of reef growth possibly explains the diversity in buildup geometry (see text for discussion).

The top of unit 4 consists of several meter-thick parasequences, which are based in heterolithic facies and grade into relatively thin, hummocky cross-stratified grainstones. Unit 5 contains a thick interval of amalgamated grainstones with hummocky as well as trough cross-stratification. Both grainstone-dominated intervals have sheetlike geometries because they accumulated during times of decreasing accommodation. Both units 4 and 5 extend far beyond the study area for over tens of kilometers (Grotzinger, 2000).

A laterally continuous thrombolite-stromatolite reef caps OS2 and immediately sits above a sequence boundary in an initial transgressive position (Figure 5) (Grotzinger, 2000). This reefal buildup was not incorporated into the 3-D outcrop models presented in this article.

DIGITAL DATA COLLECTION

Traditional field observations, including sedimentologic, facies, and sequence-stratigraphic observations, were integrated to create a detailed sedimentologic and sequence-stratigraphic framework for the terminal Proterozoic carbonate ramp system of the Kuibis Subgroup

(Smith, 1998; Grotzinger, 2000). Figure 6 illustrates the coarsening-upward shoaling sequence of OS2 with intervals dominated by heterolithic-, grainstone-, or thrombolite-stromatolite reef facies. These major depositional elements of OS2 were mapped with digital field techniques that are described below.

Digital Data Acquisition System

Real-time kinematic global positioning system (RTK GPS) receivers (Trimble 4700 GPS receiver) and a total station (Trimble TTS-300 total station) were used to collect 3-D digital geologic data. The total station can make laser distance measurements with or without surveying reflectors, depending on outcrop accessibility and distance to target. Using positions of known benchmarks collected with the GPS system and stored on the data collectors, the distance measurements made with the total station can be put directly in real-world coordinates. The spatial measurements from both the GPS and total station systems are corrected by a GPS base station in a known fixed location, resulting in a relative positional accuracy of approximately 2–5 cm (0.78–2 in.) horizontally and 5–10 cm (2–4 in.) vertically. Static

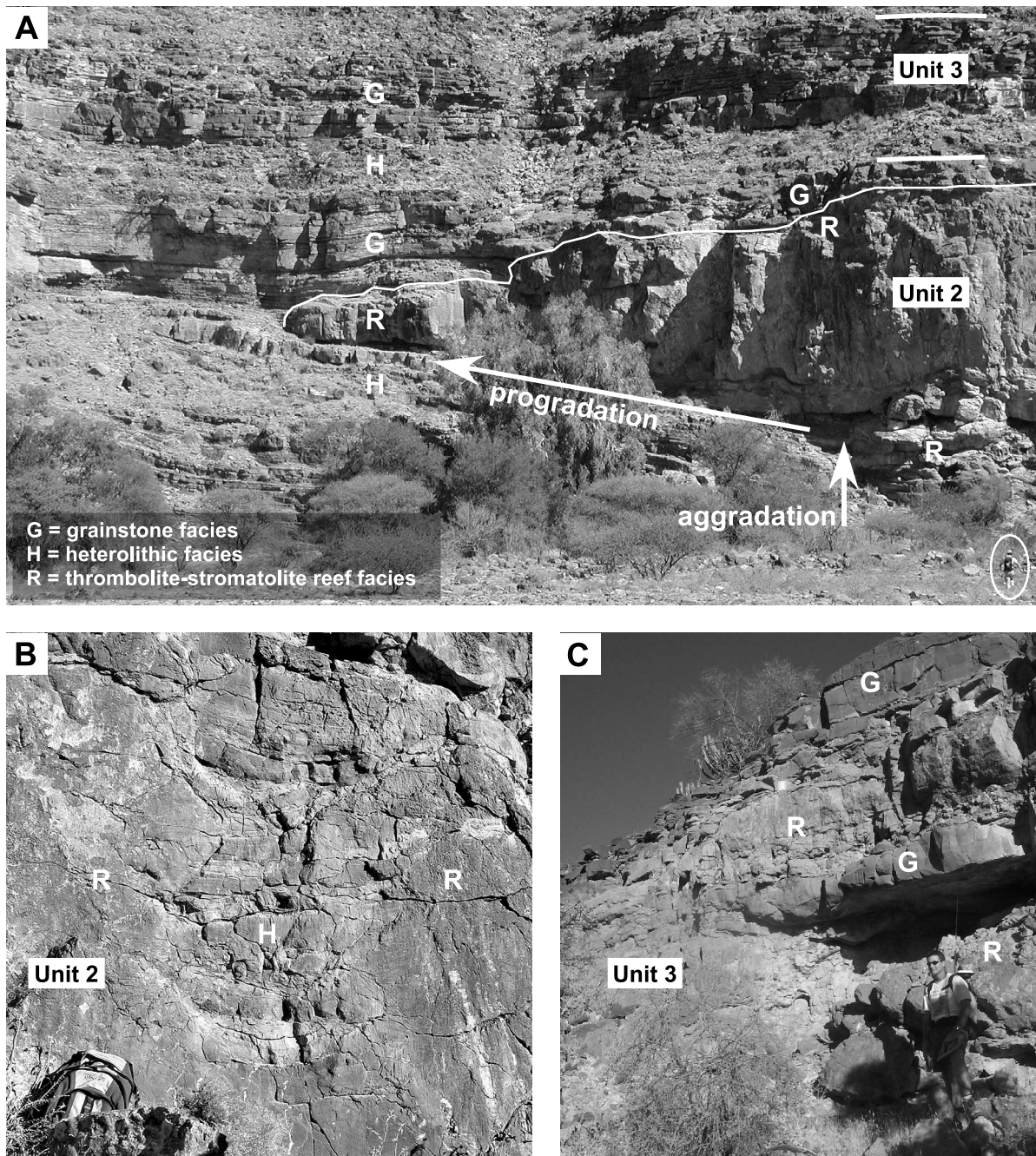


Figure 8. Outcrop photographs showing architectural elements of reefal buildups. (A) The development of buildups started with an aggrading phase, during which they were associated with heterolithic facies (H). As accommodation space decreased, the thrombolite-stromatolite reefs (R) prograded and became associated with grainstones facies (G). Grainstone deposition completely covered the reefs during the final stage of the sequence-stratigraphic unit. (B) Thrombolite-stromatolite reefs (R) with an in-between heterolithic fill (H) illustrating aggradation. (C) Photograph illustrating the contemporaneous association of grainstones (G) and thrombolite-stromatolite reef facies (R).

GPS measurements are collected at the GPS base station to attain an absolute positional accuracy (i.e., in world map coordinates) of approximately 20 cm (8 in.) for the data set presented in this article (Hurn, 1993).

Data Collection

An area of approximately 20 km² (7.7 mi²) was mapped (Figure 3), and approximately 60,000 data points were collected. We mapped the stratigraphic

and depositional contacts of interest (the top and base of grainstone units; the outline of reefs) by physically walking and recording data points normally every 2 m (6.6 ft). The data points were stored in a data collector (Trimble TSC1 data collector). Different geologic features being mapped are identified by assigning different values to attributes (e.g., kind of sedimentary facies, lithology, sedimentary structure, stratigraphic-surface type) that are associated with the spatial location of each data point.

One can directly measure stratigraphic sections using the GPS and total station as long as the lithological, sedimentologic, or stratigraphic units are thicker than the spatial precision of the measurement system; in our case, this would be suitable for measurements more than 5 cm (2 in.) apart. One need only correct for local structural dip to obtain stratigraphic thickness. By simultaneously mapping lithologies above and below a contact, one can effectively measure stratigraphic sections along stratal boundaries. For the petroleum industry, this would be similar to geosteering along a stratigraphic contact. This way, one can directly obtain information on facies changes or lateral dimensions of geological bodies.

At the end of each work period, the collected data were downloaded from the data collector to a standard personal computer. Data were assembled, edited, and regrouped using geographic information systems (GIS) software (Trimble Geomatics Office). Data were exported from the GIS software in spreadsheet files for input to the geological modeling software.

Digital Elevation Model

A 3-D digital elevation model (DEM; spatial resolution of 10 m [33 ft]) was created using photogrammetric techniques that combine aerial photographs with high-precision GPS data as control points (Lillesand and Kiefer, 2000). Scanned orthophotographs with 1 × 1-m (3.3 × 3.3-ft) pixel size were superimposed on the DEM (Figure 3B). The accuracy of the DEM only resolves major lithological boundaries. Not all stratigraphic contacts were mapped continuously over the entire area because of outcrop conditions and time constraints. Nevertheless, plotting collected data points as a reference on the DEM allowed digital interpolation to fill data gaps of major features recognizable on the aerial photos and DEM. These interpolated data points were added to the data set.

Remote surface mapping has been applied successfully and proved to be efficient (cf. Adams et al., 2004; Banerjee and Mitra, 2004).

Data Visualization and Modeling

For building 3-D outcrop models, we used a personal computer-based, 3-D modeling software package Petrel™ (a trademark of Schlumberger Limited) (e.g., Blendinger et al., 2004). Both the DEM and collected data were transferred to the modeling package. Three-dimensional visualization of the high-resolution DEM, together with collected data, allowed us to view and analyze data in the field and served as feedback for subsequent mapping. Both deterministic and stochastic methods were used to model the observed stratigraphy. We describe the details of the modeling processes and the creation of the 3-D outcrop models in a subsequent section of the article.

Spatial Data

A unique advantage of using digital field techniques is the ability to rapidly extract quantitative spatial data from digital data sets, which can be used as input to quantitative 3-D geological models. For example, the dimensions of sedimentary bodies (e.g., carbonate build-ups) or length scales of geometrical relationships defined by lithofacies or stratal boundaries can be obtained directly.

3-D OUTCROP MODEL BUILDING

The architectural elements encountered in the field and the sequence-stratigraphic framework are shown schematically in Figures 5 and 7. Generally, all the stratigraphic and depositional contacts that were needed to reconstruct the stratigraphy were mapped, for example, the top and base of grainstone-dominated units; the reefs were mapped by physically walking their outlines (Figure 7). A digital data set, containing spatial coordinates of the contacts and associated geological attributes, was compiled and used for 3-D model construction. The first step in 3-D model building is the creation of the structural framework or grid, i.e., creating surfaces that define the mapped stratigraphic and depositional contacts (Krum and

Johnson, 1993; Kerans and Tinker, 1997; Grötsch et al., 2003; Larue and Legarre, 2004). Both deterministic and stochastic methods were used to create these surfaces.

Deterministic Modeling of Continuous Units

Modeling continuous, sheetlike stratigraphic and depositional surfaces was relatively straightforward. Interpolation between and extrapolation beyond data points collected along canyon walls were done by fitting surfaces with a minimum curvature algorithm. Figure 9 shows the procedure for the reconstruction of unit 3, i.e., the thrombolite-stromatolite reef with tabular morphology that interfingers with grainstones. The basal grainstone unit on which the reef initiated was mapped along the canyon walls, and subsequently, a surface representing the top of this unit was constructed (Figure 9A, C). A surface representing the top of the reef was constructed in the same way; the margin of the reef was modeled by projecting the top reef surface vertically onto the basal grainstone unit (Figure 9B, D). Finally, a surface was modeled representing the top of the contemporaneous grainstone unit (Figure 9E). All other continuous, flat-topped units, such as units 4 and 5, were modeled in a similar fashion.

Not all stratigraphic contacts that are needed to reconstruct the geology of the carbonate ramp were mapped in the field. Stratigraphic sections were measured (Figure 5) and provided a control, after correcting for structural dip, on the thickness variation of several units. For example, only the top of the grainstone bed onto which the tabular-shaped buildup of unit 3 developed was mapped (Figure 7). The base of this bed was obtained by duplicating the top surface and translating it 1.5 m (5 ft) vertically downward.

Statistical Characterization and Modeling of Discontinuous Reefal Bodies

Stochastic object modeling was performed to create a surface representing the discontinuous, oblate dome-shaped thrombolite-stromatolite reefs of unit 2 (Figure 7). First, the widths and heights (i.e., height of the final geometry in cross section as observed in outcrop and not synoptic relief) of the observed and mapped reefal buildups were computed. Subsequently, a correction was applied to transform the two-dimensional (2-D) outcrop measurements to 3-D. Fi-

nally, surfaces were realized using the width and height distributions as input. A detailed description for the statistical characterization of the dome-shaped reefs and the construction of surfaces representing envelopes of unit 2 reefal buildups is discussed below.

Data Acquisition

We mapped the reefal buildups by physically walking out two surfaces: (1) the basal contact onto which the thrombolite-stromatolite reefs developed; and (2) the reefal outlines, i.e., the line marking the lateral or vertical termination of the reefal buildup (Figure 10A). The raw data are lists of 3-D coordinates, with one list indicating the buildup outline and a second list representing the basal contact. These two lists were combined and sorted to obtain one list of data points that describes the buildups and, when absent (i.e., when a gap in between buildups is present), the basal contact onto which the buildups developed (Figure 10B). A surface representing the basal surface was constructed deterministically with the data points collected along the basal contact (Figure 10B). Finally, the basal surface elevations were subtracted from the elevations of the data points in the combined list of similar map (x, y) locations, so that $z = 0$ corresponds to a contact with the basal surface. The data set is not corrected for structural dip because this would require many local dip measurements; not correcting for structural dip is a reasonable assumption given the scale of the buildups (several meters high; see Figures 8A, 10A) and minor structural dip (see Figure 3).

Measuring Width and Height Distributions

Statistics about two categories of reefal buildups were compiled. Buildups of group 1 represent the discontinuous thrombolite-stromatolite reefs with dome-shaped morphology that developed on top of the basal surface; group 2 represents buildups that developed on top of group 1 buildups. In other words, the location of buildup development discriminates groups 1 and 2 buildups (Figure 10). Statistics regarding the distribution of buildups in width and height were computed in several steps. First, the combined and sorted list (Figure 10B) was mapped from 3-D to 2-D, where the first (horizontal) coordinate represents the vertically projected arc length s along the curve, and the second (vertical) coordinate is identical with the z -coordinate values (Figure 10C). In what follows, this function is denoted by $z = q(s)$. The local maximums and minimums along the curve are then tabulated

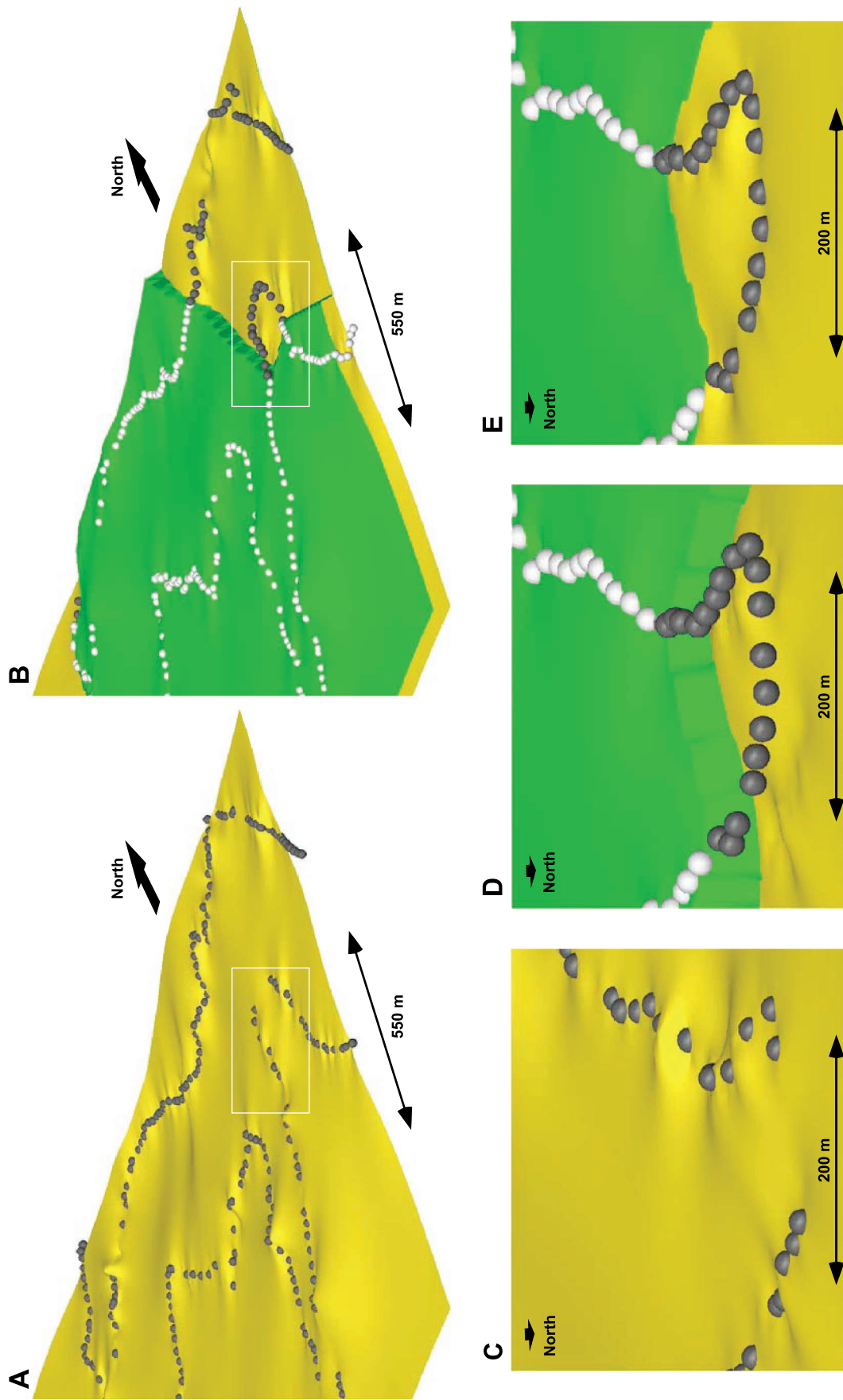


Figure 9. Images illustrating the surfaces reconstructed for unit 3. Vertical exaggeration is 5 for all images. (A) The basal grainstone unit on which the reef initiated was mapped along the canyon walls (gray dots are collected data points). Subsequently, interpolation between and extrapolation beyond data points collected along canyon walls was done by fitting a surface with a minimum curvature algorithm. (B) A surface interpolated between data points mapped on top of the reef (white dots). (C) Detail and close-up of surface illustrated in (A). (D) Detail and close-up of the surface illustrated in (B). The margin of the reef was modeled by projecting the top reef surface vertically onto the basal grainstone unit of (A). (E) The last surface that was created represents the top of the contemporaneous grainstone unit.

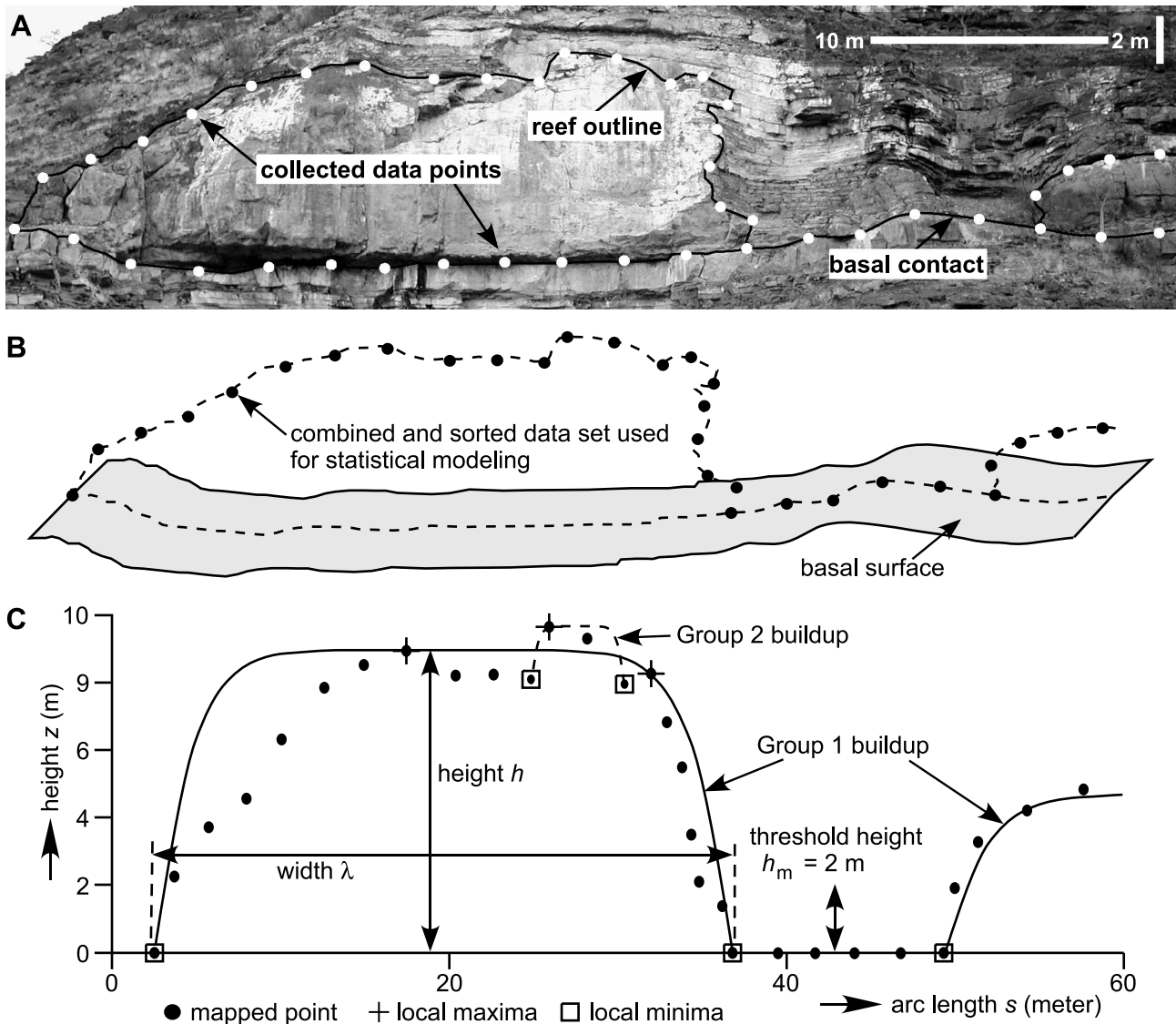


Figure 10. Methods of measuring buildup height and width. (A) Outcrop photograph of an oblate dome-shaped buildup of unit 2 in cross section (see Figure 6A for location). White dots indicate hypothetical data points collected along the outline of the buildup and basal surface. (B) Combined and sorted data set (black dots connected by dotted line) describing the buildups and, when absent, the basal contact. The gray surface represents the basal surface and was constructed deterministically. (C) Data set (black dots) with $z = 0$ corresponding to the basal surface. The horizontal coordinates are plotted as the vertically projected arc length s along the curve. Local maxima and minima are tabulated according to changes in the sign of the first derivative in elevation with respect to s . See the text for a discussion on width and height calculations. The buildup outlines representing group 1 (solid lines) and group 2 (dashed line) are hypothetical realizations.

according to changes in the sign of the first derivative in elevation with respect to s (Figure 10C). Statistics about the two groups were compiled while tracing $z = q(s)$, i.e., while stepping through the list of spatial-ordered data points. The starting point was a local minimum that lies below a threshold height h_m . The threshold height is set to $h_m = 2$ m (6.6 ft) because points are recorded with the GPS at 2-m (6.6-ft) separations (i.e., total distance in 3-D). As a result, narrow

gaps separating buildups shorter than 2 m (6.6 ft) are not measured, and all other gaps can be resolved. When a local maximum was encountered that lies above h_m , the next local minimum that lies below h_m was searched. The distance between the first and second below-threshold local minimum (which lie to either side of at least one above-threshold maximum) indicates the measured width λ of a group 1 buildup in cross section (Figure 10C). The mean of local

maximums encountered between these minimums was recorded as the cross sectional buildup height h (Figure 10C). The widths of group 2 buildups were obtained by measuring the distances between above-threshold local minimums that occur on a group 1 buildup (more than one local minimum is needed on a group 1 buildup to have a group 2 buildup). The distance between a local maximum and the preceding local minimum gives the height of a group 2 buildup (Figure 10C).

Figure 11A shows the sampled probability density (circles) and a spline fit (solid curve) sampled at 5-m (16-ft) intervals for measured widths λ of group 1 buildups along the canyon wall. This function was

obtained as follows. First, the list of measured widths was sorted in order of increasing size. The first 15 points were averaged to calculate a mean width $\bar{\lambda}$. The minimum value in this group of 15, when subtracted from the maximum value, gives a range $\delta\lambda$. The density for these 15 points is then $15/\delta\lambda$ and is plotted at the point $\bar{\lambda}$. This calculation was carried out for points 2–16 and then 3–17 and so on. This number density curve was then rescaled, so that the area beneath the curve is equal to 1, such that the result is a properly normalized probability-density function. The same procedure was repeated to obtain density functions for measured cross sectional heights (spline fit sampled at 0.1-m [0.33-ft] intervals) for group 1 buildups

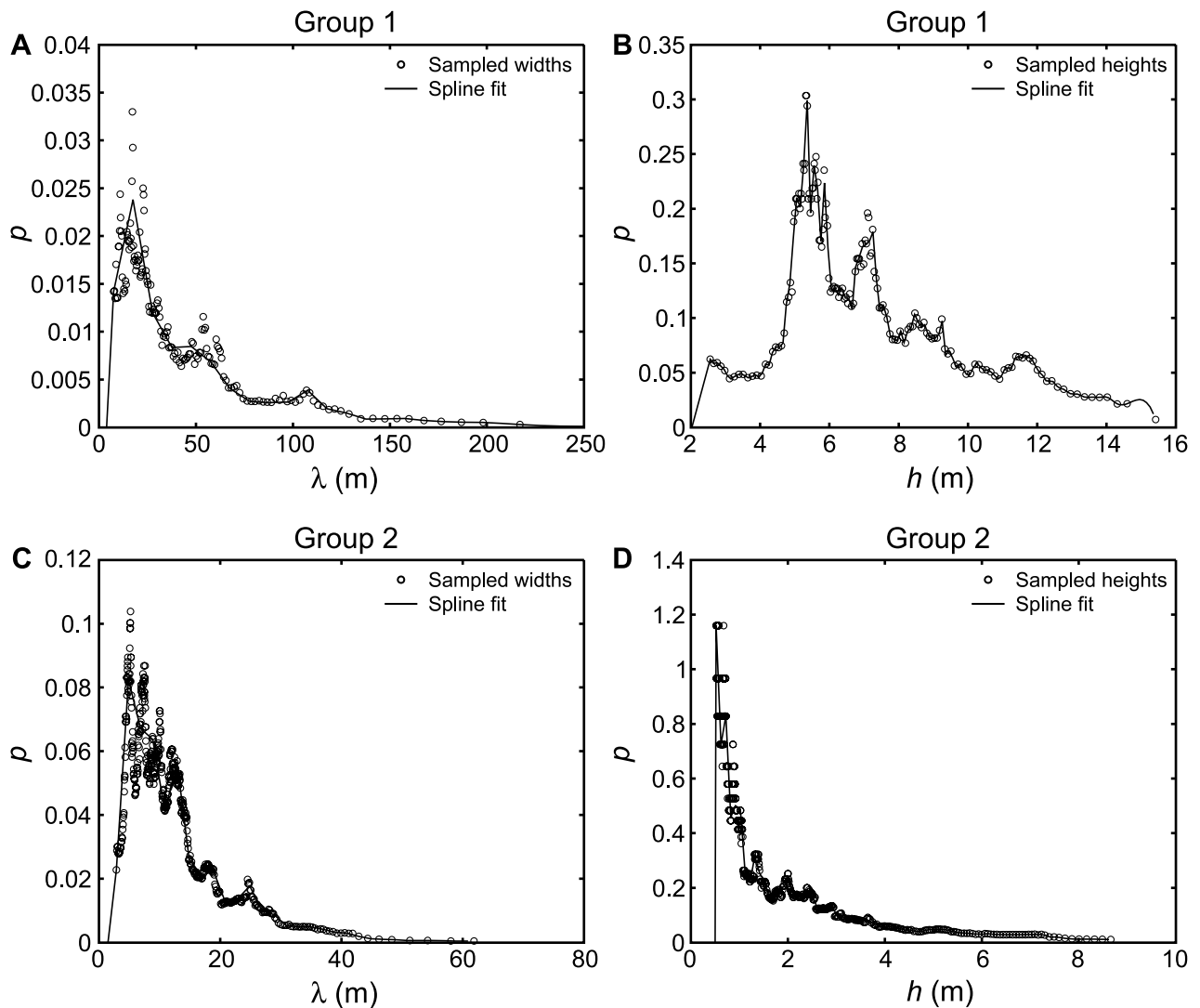


Figure 11. Sampled probability density (circles) and spline fit (solid line) for widths or heights of cross sections through group 1 and group 2 buildups measured along the canyon wall. (A) Widths of group 1 buildups; (B) heights of group 1 buildups; (C) widths of group 2 buildups; and (D) heights of group 2 buildups.

(Figure 11B), as well as widths and heights for group 2 (Figure 11C, D).

In addition to height and width, it is also a simple matter to measure the orientation of buildup cross sections along the canyon wall. Figure 12 is a plot of the cross sectional widths versus orientation for all group 1 buildups in our data set. The absence of any correlation is consistent with an absence of elongation along a preferred direction, and therefore, the buildups are inferred to be circular in plan view. However, in the field, this circular plan-view shape can be observed directly; in some cases, the canyon provides 3-D cuts, allowing the observation of an almost complete isolated buildup.

Correcting Measured Distributions

We compiled the statistics for buildup widths from 2-D cross sections (i.e., measured along the canyon walls), and for that reason, spatial correction of these measured distributions was necessary to estimate the distribution of actual buildup widths in 3-D. The reefal buildups have steep margins, and therefore, the measured height distributions do not require correction. The width correction process involved two steps.

First, a correction was applied to determine the distribution of actual buildup widths intersected by the cross sections. Buildups are assumed to be circular in plan view (see Figure 12). If a series of equally probable arbitrary cuts are made through a circle of diameter Λ , a distribution of the width of cross sections λ is obtained (the cuts do not have to pass through the center of the circle). Letting $l = \lambda/\Lambda$, we

can write this as a probability-density function $p(l)$. It is a simple exercise to show that this function is given by

$$p(l) = \frac{l}{\sqrt{1-l^2}} \quad (1)$$

By integrating $lp(l)$ from $l = 0$ to $l = 1$, the mean value \bar{l} for this distribution is $\bar{l} = \pi/4$. As a consequence, the measured cross sectional widths are, on average, a fraction $\pi/4$ of the true width. If the probability-density function of measured cross sectional widths c is referred to as $p(l)$, then a rough approximation can be made of the distribution of true widths $p(\Lambda)$ by letting $p(\Lambda) = (1/N)p(4\lambda/\pi)$, where N is a normalization constant. In other words, the λ axis of the probability-density function was rescaled by a factor $4/\pi$ to produce an estimate $p(\Lambda)$ of the probability-density function as a function of the actual buildup widths (Figure 13). It is more correct to obtain the probability-density function for Λ using the Bayes theorem (e.g., White and Willis, 2000) and the joint probability density for λ and Λ (the measured and actual widths, respectively), but this requires additional information about the distribution of Λ .

To obtain a probability-density function for the widths of buildups distributed throughout unit 2, a second correction considers the larger frequency of occurrence of smaller objects. In particular, in going from 2-D to 3-D, the relative frequency of a particular length class will decrease in direct proportion to its length (cf. Geehan and Underwood, 1993)

$$p_{3-D}(\Lambda) = \frac{p(\Lambda)/\Lambda}{\int_0^\infty p(\Lambda)/\Lambda d\Lambda} \quad (2)$$

Figure 13A and B show plots of $p(\lambda)$, $p(\Lambda)$, and $p_{3-D}(\Lambda)$ for groups 1 and 2, respectively.

Realizing a 3-D Surface of Reefal Buildups

A statistical realization of a 3-D surface that forms the upper boundary of the reefal buildups of unit 2 is created by sampling values from the height distribution and the corrected width distribution (Figure 13) using the von Neumann rejection technique (von Neumann, 1951). The correlation between height and width for group 1 buildups can be seen in a plot of h versus Λ (Figure 14) (von Neumann, 1951). Zones in this plot are present in which no buildups occur (i.e., certain proportions are precluded). In the region between these zones, the probability of any proportion is roughly the

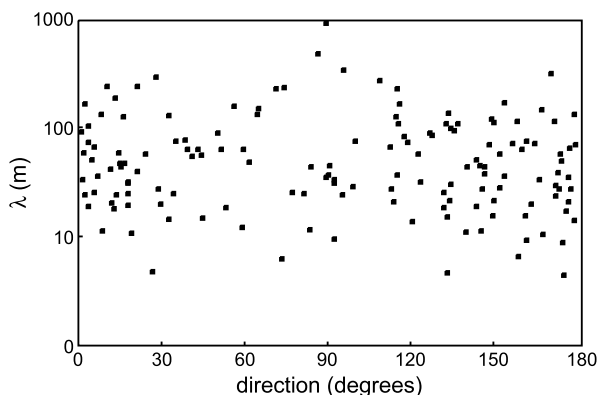


Figure 12. Plot of cross sectional widths versus orientation for all group 1 buildups in the data set (of which 150 are present). The absence of any correlation is consistent with the absence of elongation along a preferred direction, i.e., the buildups are circular in plan view.

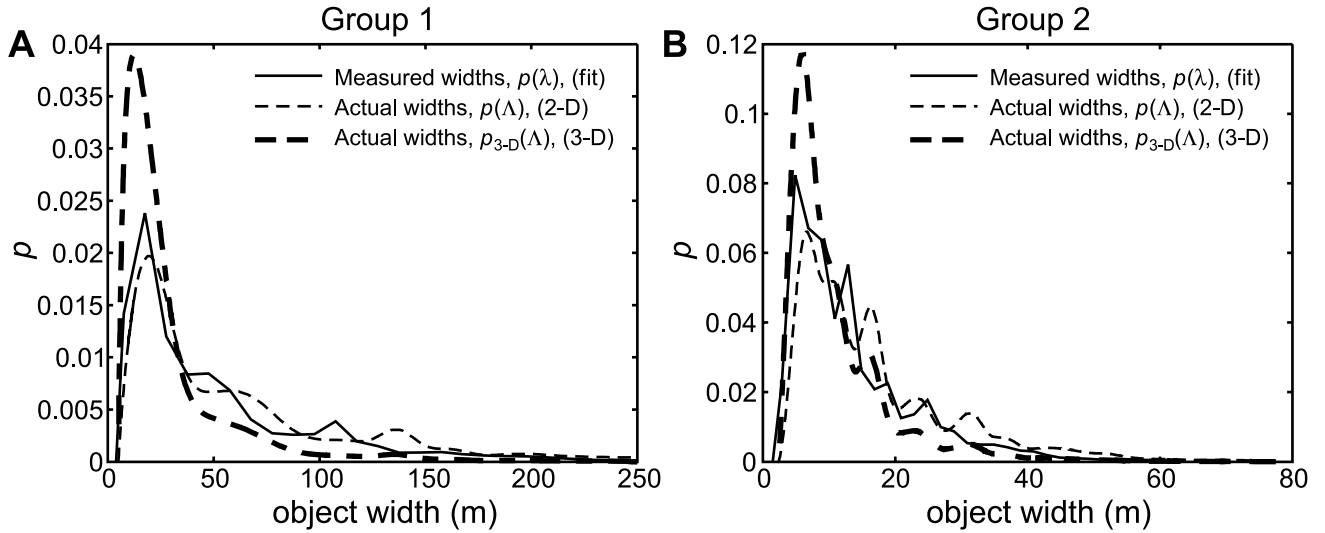


Figure 13. Spline fit to sampled probability density (solid line) and corrected curves for approximating the actual width distribution of buildups in cross section (dashed line) and within unit 2 (bold dashed line). (A) For the case of group 1 buildups; (B) for the case of group 2 buildups.

same. We have assumed that any height h may be paired with any width λ , in the case where $h \geq 1 + 0.0335\lambda$ and $h \leq 13 + 0.0335\lambda$ (see Figure 14). In the case of group 2 buildups, we assumed that any height in the measured distribution could be paired with any width.

The upper surface of a single buildup can be described by means of the following equation, letting $\delta r \equiv \sqrt{(x - x_0)^2 + (y - y_0)^2}$:

$$f(x, y) = H(h(1 - [(2/\lambda)\delta r]^\gamma)) \quad (3)$$

where H is the Heaviside function [i.e., $H(x) = x$ for $x \geq 0$, and $H(x) = 0$ otherwise]; h is the height of the buildup; λ is its width; x_0 and y_0 indicate its position; and γ is a measure of the steepness of its flanks. As γ increases, the shape tends toward that of a cylinder. We always used $\gamma = 8$; a vertical cross section illustrating this shape is illustrated in Figure 10C.

Buildups belonging to group 1 are added by means of the following equation

$$g_{n+1}(x, y) = g_n(x, y) + H(g_n(x, y) - f(x, y)) \quad (4)$$

where H is the Heaviside function; $f(x, y)$ is given by equation 3; and n is the state of the surface immediately before and $n + 1$ immediately following the addition of the buildup described by $f(x, y)$. That is, the group 1 buildups were not superposed: two buildups of the same height placed in the same location using equation 4 would result in no change. Group 1 build-

ups were placed on an initially horizontal surface. When a new buildup was added, its position (x_0, y_0) was chosen at random from a uniform distribution. If the new buildup overlaps a previous buildup, then a new position was selected until no intersections occurred. If, after 100 attempts, a new buildup of a given height and width could not be placed on the surface, then it was placed wherever it landed on the 101st attempt. In our realization, fewer than 5% of buildups were added to the surface in this manner.

The linear coverage or linear density of buildups is measured from curve $z = q(s)$. The fraction of the

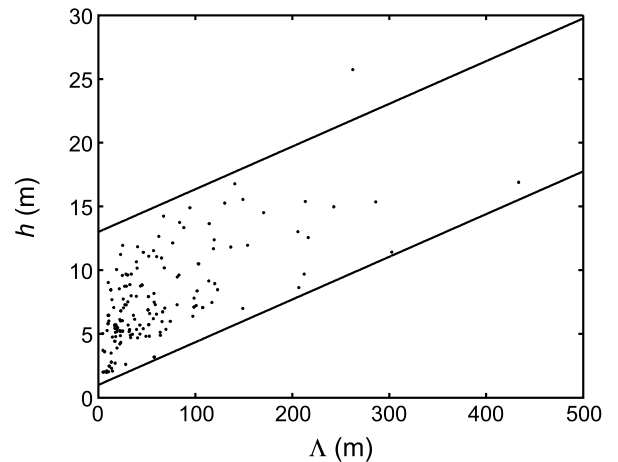


Figure 14. Heights versus widths of group 1 buildups. See text for the discussion.

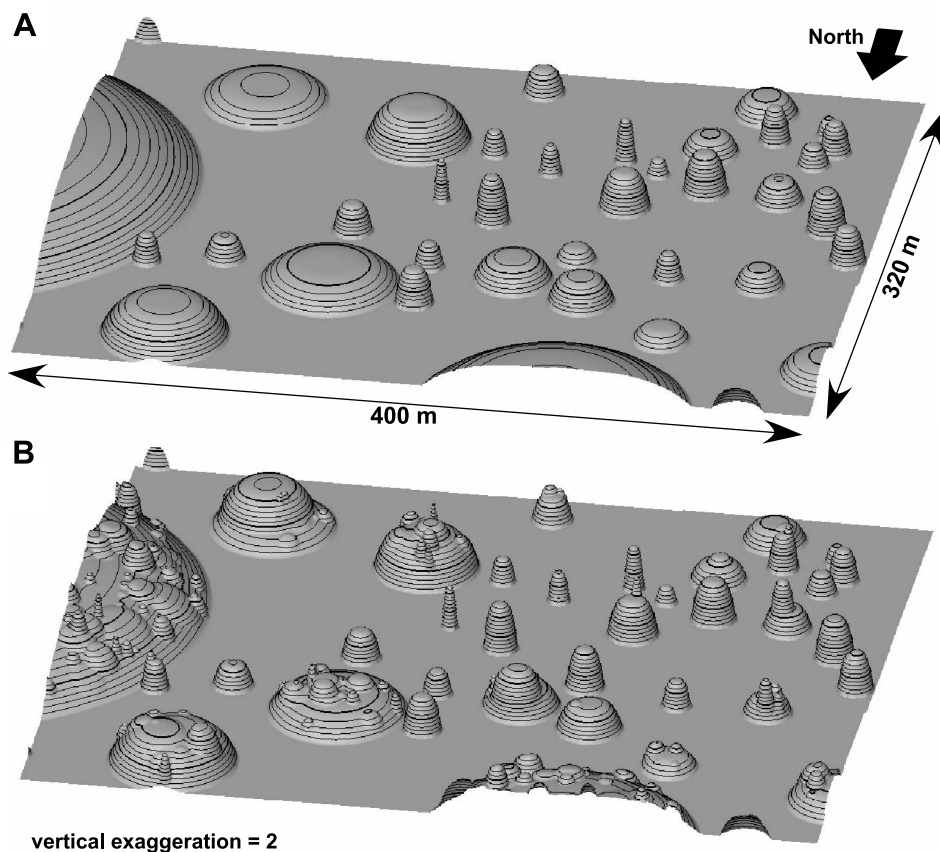
length of this curve that was occupied by group 1 buildups is 0.45. As group 1 buildups are added to the surface, the linear density along five parallel lines (spaced at intervals that are large with respect to the average size of buildups) were calculated and averaged. When this average exceeded 0.45, the calculation stopped, and the group 1 surface was completed. An example is shown in Figure 15A.

Group 2 buildups represent roughness elements on the surfaces of group 1 buildups. The distribution of heights is truncated below $h = 0.50$ m (1.6 ft) because this is roughly the length scale associated with the condition and limitation of the outcrop (i.e., the resolution with which loose blocks versus solid outcrop can be resolved). Group 2 buildups were added to a fresh surface using equation 4 only in those regions where group 1 buildups reside. Group 2 buildups were added until 50% of the group 1 surface was covered by group 2 buildups. Because of computational limitations, no attempt was made to avoid the overlap of group 2 buildups. The resulting group 2 surface was then superposed on the group 1 surface to produce the result shown in Figure 15B.

Model Construction

The reconstruction of architectural elements and especially that of the geometrically diverse reefal buildups is the most important step in the model-building process. Unit 2 dome-shaped buildups (i.e., group 1 buildups) have variable dimensions with an average size of 10–20 m (33–66 ft) wide and 5–8 m (16–26 ft) high (Figures 11, 13). Roughly, the buildup width is two times greater than the height. The buildups are circular in plan view as observed in the field and illustrated by the data (Figure 12). We did not analyze whether a pattern in the distribution of buildups exists, i.e., change in dimensions from updip to downdip. The density with which the buildups cover the basal surface was estimated to be around 45%. The buildups that developed on top of group 1 buildups have an average width of 5–10 m (16–33 ft) and variable height with a maximum of up to 6–8 m (19–26 ft). Just as group 1 buildups, the buildup width is two times greater than the height. The increase in volume obtained by the addition of group 2 on top of group 1 is about 7% (see Figure 15).

Figure 15. Resulting surfaces representing the isolated dome-shaped buildups of unit 2. Surface grid spacing for both images is 1×1 m (3.3×3.3 ft). (A) Group 1 surface. (B) Final surface as a result of summing the group 2 surface with the group 1 surface.



The margins of the tabular-shaped buildup were all mapped, and the constructed model illustrates the minimum size for the reef. The reef is approximately 3 km (1.8 mi) along the dip direction; it is roughly 1.5 km (0.9 mi) wide in the strike direction of the carbonate ramp. The thickness of the reef ranges from 10 to 15 m (33 to 49 ft).

The surfaces (or grids) that represent various stratigraphic contacts were used to construct a 3-D stratigraphic outcrop model. The 3-D model was built with Petrel™ software, which allows the characterization of the type of stratigraphic contact present, e.g., surfaces can be conformable or erosional. Figure 16 illus-

trates the model-building process for unit 2. Most surfaces have a conformable relationship. However, the reefal buildups were not allowed to be higher than the surfaces representing the overlying grainstone unit; the surface settings were changed accordingly. The final 3-D outcrop model is illustrated in Figure 17. No further subdivisions have been made, and internal layering has not been applied to the lithologic and stratigraphic units. The resolution of the model is already very high. Figure 17B shows the horizontal grid spacing of 10 m (33 ft) and the vertical subdivision of the model by the surfaces. However, one can easily imagine incorporating fine meter-scale

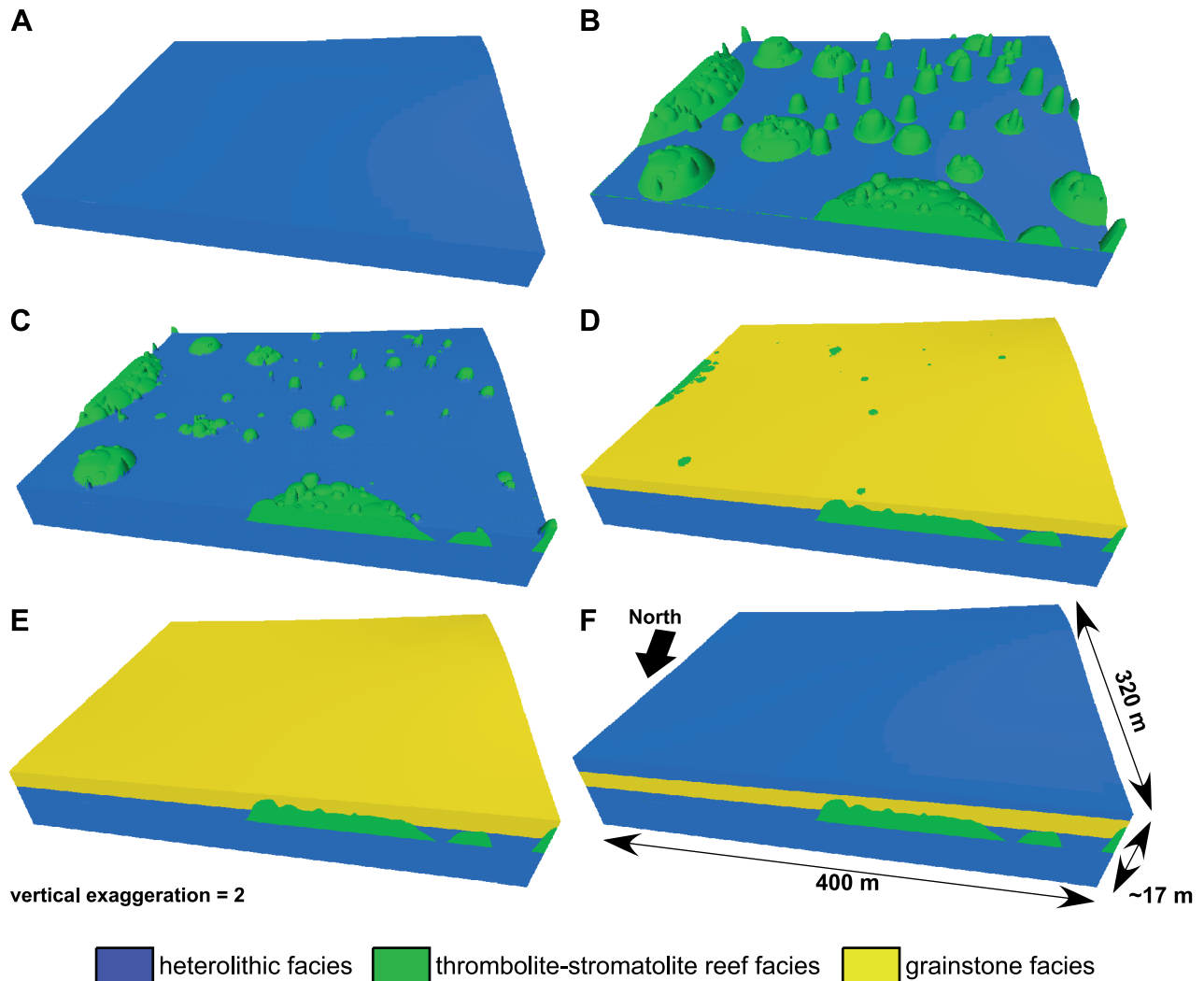


Figure 16. Images illustrating the model building of unit 2. Only images (A), (E), and (F) can be regarded as time slices. (A) Basal heterolithic unit. (B) Model for the dome-shaped buildups with final geometries. (C) Heterolithic interval associated with the early stages of reef development. (D) Grainstone facies associated with the final stage of reef development. (E) Grainstone facies related to the final stage of unit 2. (F) Heterolithic base of unit 3.

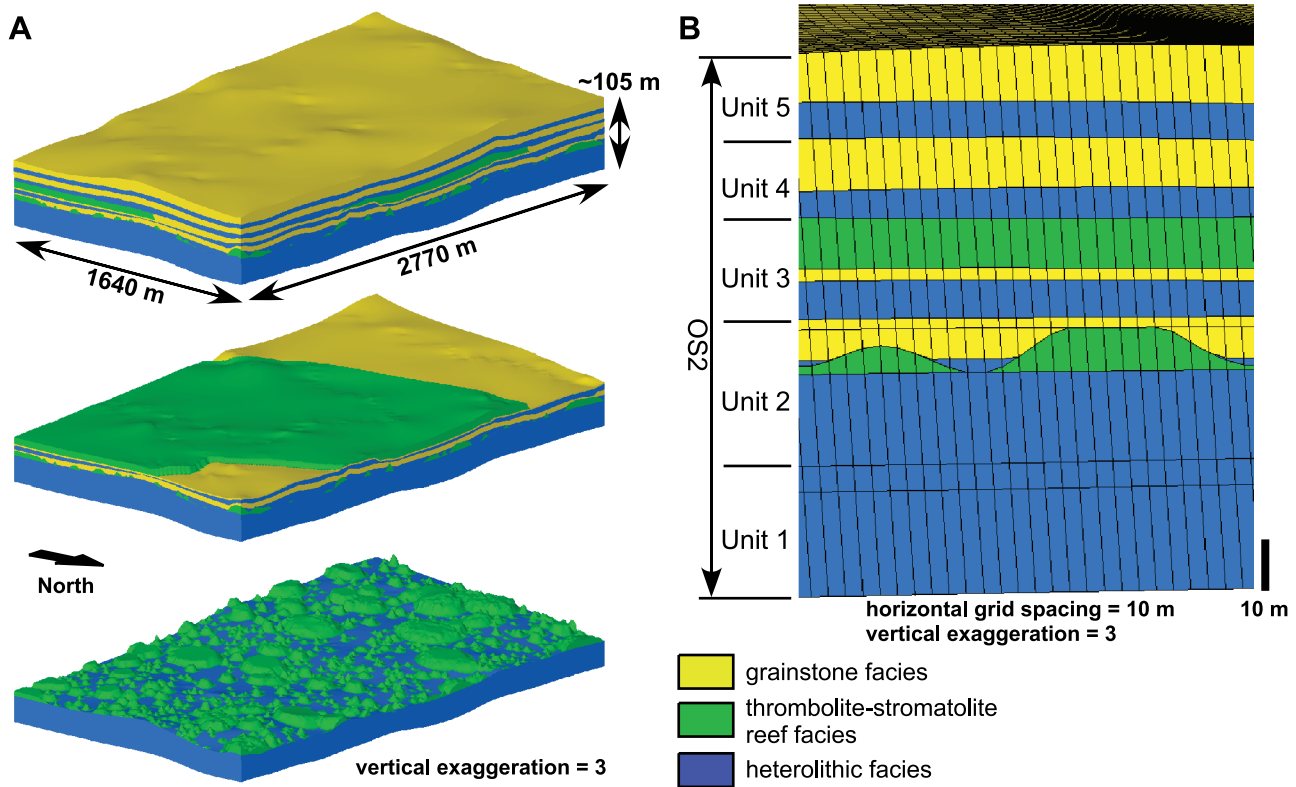


Figure 17. (A) Final 3-D outcrop model. The dome-shaped thrombolite-stromatolite reefs of unit 2 (lower image) and the tabular-shaped buildup of unit 3 (middle image) are illustrated separately, but note that these two images do not represent time slices. For the location of the model, see box in Figure 3. (B) Cross section through 3-D outcrop model illustrating the stacking of the five units of OS2. For comparison, see outcrop image of Figure 6. Horizontal grid spacing is 10 m (33 ft); vertically, the model is subdivided by stratigraphic and depositional surfaces.

layers into the model, especially because stratigraphic sections provide meter-scale lithological and sedimentological details.

We populated the model with the dominant facies observed in the field, i.e., grainstone, heterolithic, or thrombolite-stromatolite reef facies (Figures 16, 17). We did not distribute petrophysical properties. Our aim was to create an accurate 3-D stratigraphic model, which was integrated with detailed rock and sedimentologic analysis, representing the carbonate ramp in outcrop.

DISCUSSION

Organization of Reefal Buildups in Carbonate Ramp Systems

Generally, in carbonate ramp depositional environments, isolated carbonate buildups develop mostly during late transgressive and early highstand systems

tracts when sediment input is reduced (Burchette and Wright, 1992; James and Bourque, 1992; Tucker et al., 1993; Dorobek and Bachtel, 2001). This is also the case for thrombolite buildups (e.g., Grotzinger, 2000; Mancini et al., 2004). Similar patterns are observed for the Kuibis Subgroup and especially for OS2, where the development of dome-shaped buildups occurred in deeper settings and tabular-shaped buildups developed in settings when accommodation was relatively lower (Smith, 1998; Grotzinger, 2000; Adams et al., 2004; this study). Similar observations have been documented in the Lower Cretaceous of New Mexico (Murillo-Muneton and Dorobek, 2003). Here, aggradational, lenticular, and symmetrical carbonate mud mounds a few to tens of meters in size and with a low syndepositional relief (<5 m; <16 ft) developed in mud-dominated outer-ramp to basin settings. Tabular buildups with widths up to several hundred meters and a height of up to 90 m (295 ft) and a minor synoptic relief were associated with coarse-grained skeletal fragments, indicating higher accumulation

rates and shallower water depths. The progressive shallowing Lower Cretaceous carbonate ramp sequence of New Mexico appears quite similar to the terminal Proterozoic Nama Group carbonate ramp system. In a carbonate ramp shoaling sequence, the following changes commonly occur: (1) buildup morphology changes from dome shaped or lenticular to tabular, (2) the associated facies becomes coarser, and (3) syndepositional relief decreases. Although this article focused on the final buildup dimensions and not on the synoptic relief of the buildups, the dome-shaped reefs tend to have a higher syndepositional relief as the tabular reefs.

Clearly, accommodation trends and sedimentation rates and, therefore, the ramp style determine the geometry and dimensions of developing carbonate buildups in carbonate ramp systems. The stratigraphic position of buildups in the framework thus has strong reservoir implications. The facies association and sequence-stratigraphic setting of buildups can probably help in determining their geometries.

Digital Field Geology and 3-D Outcrop Modeling

A combination of sequence-stratigraphic, sedimentologic, and facies analysis resulted in a detailed sedimentologic and sequence-stratigraphic framework for the terminal Proterozoic carbonate ramp of the Nama Group (Smith, 1998; Grotzinger, 2000; Adams et al., 2004). These conventional mapping methodologies were complemented with digital surveying tools to acquire a digital data set of surveyed data points, mapped at meter scale, integrated with the DEM and projected aerial orthophotographs. Although the qualitative understanding of the gross stratigraphic development was not enhanced by digital mapping, the digital field techniques enabled rapid quantitative mapping, simplified 3-D outcrop model construction, and allowed high-resolution quantitative measurement of key sedimentological elements (e.g., the statistical distribution of reefal buildups). The geometric relationships also are depicted and corrected more accurately.

Our study presented the quantification of reefal buildups in a ramp system by digital mapping. The ability to quantify spatial characteristics and length scales accurately is very significant. Without the ability to obtain spatial information on buildup dimensions, we could not stochastically model the stratigraphic interval dominated with discontinuous dome-shaped

thrombolite-stromatolite reefs (unit 2; Figures 7, 16). Although spatial data can be obtained from photo mosaics and direct measurements in the field, the ease and resolution with which this kind of data can be extracted from the digital data set contrast starkly with traditional mapping techniques.

The digital data were direct input for static model building. A combination of deterministic and stochastic modeling techniques allowed the reconstruction of the major stratigraphic and depositional contacts. The final 3-D outcrop model contains precise information of the architecture and organization of the geometrically diverse thrombolite-stromatolite buildups. Subsequently, the model could be populated with petrophysical properties, or the model units could be refined with fine, meter-scale layering to create a static property model on which dynamic reservoir-simulation modeling can be conducted.

Subsurface Implications

The detailed digital mapping of the major depositional elements in the study area has enabled us to characterize quantitatively the stratigraphic architecture of the carbonate ramp system and make this outcrop example a useful database for analogous subsurface petroleum reservoirs. Although subsurface analogs of the same age are sparse, examples from Oman have been documented (Mattes and Conway Morris, 1990; Grotzinger and Amthor, 2002; Amthor et al., 2003; Peters et al., 2003; Schröder et al., 2003). The Ara Group of Oman contains carbonate-evaporite sequences in which the carbonate rocks are interpreted to have platform geometries ranging from low-gradient ramps to rimmed shelves. The rocks contain thrombolite-stromatolite buildups and have similar facies associations as the Nama Group rocks. In addition, the age is the same and is based on biostratigraphy, chemostratigraphy, and geochronology (Amthor et al., 2003; Schröder et al., 2003). The reservoirs in Oman are dominated by grainstones and thrombotic reefs, associated with nonreservoir mudstones, that collectively form carbonate ramps (Grotzinger and Amthor, 2002).

The implications for subsurface reservoirs, which can be drawn from our study, all relate to the stratigraphic organization of the thrombolite-stromatolite reefs. Subsurface issues such as volumetric assessment and reservoir continuity and connectivity can be assessed and tested. In our case, the heterolithic facies

are analogs for the nonreservoir units in Oman; both grainstone and thrombolite-stromatolite reef facies exhibit good primary porosities and can be regarded as reservoir units in the Oman situation.

Volumetric Calculations

All units, with the exception of unit 2, are uniformly thick, laterally continuous, and exhibit minimum lateral and vertical facies variability. For example, the highstand systems tract of unit 3 consists of amalgamated beds of hummocky cross-stratified grainstones that interfingered with a tabular-shaped thrombolite-stromatolite reef. Combined, the grainstones and thrombolite-stromatolite reefs can be treated as a single, continuous reservoir unit. The same argument is applicable to units 4 and 5. The relative homogeneity of facies in these units is primarily attributed to the lack of significant amounts of intercalated heterolithic intervals. For the purpose of volumetric calculation, each of these units can be treated as a single homogenous reservoir zone.

However, unit 2 consists of dome-shaped buildups exhibiting variable dimensions that are laterally separated by heterolithic facies and capped by continuous grainstone beds. This is the most heterogeneous unit in the whole system. The lateral facies variability displayed by this unit has a profound impact on volumetric calculation. A uniform calculation of the volumetrics of unit 2 will give an erroneously optimistic value for the reef facies. In our case, the heterolithic facies interbedded between reefal facies occupy roughly 25% of the total volume of the top of unit 2; the percentage of volume occupied by reef facies and interbedded plus overlying grainstone facies is 20% and 55%, respectively (Figures 16, 17). As illustrated in this article, a more accurate way to calculate volumetrics is by understanding the spatial distribution of the reefs. The stochastic modeling approach presented in this article gives an example of how the spatial distribution of dome-shaped reefs scattered randomly within a stratigraphic unit can be approximated.

Reservoir Continuity and Connectivity

All units have a highstand systems tract dominated by grainstone facies commonly interbedded with mudstones, siliciclastic shale, and irregular laminite, forming parasequences several meters thick each. These grainstone-dominated parasequences exhibit minimum facies variability both laterally and vertically, are uniformly thick, and are laterally continuous over the entire study area. Horizontal connectivity is ex-

pected to be good; however, because of the presence of interbedded heterolithic facies, vertical connectivity may be moderate.

The oblate dome-shaped buildups of unit 2 have various dimensions and do not represent a continuous reefal buildup because the space in between buildups is occupied by heterolithic facies. However, the buildups are capped by a continuous grainstone unit. This architecture is present over the entire study area. Lateral connectivity can be impeded by the presence of heterolithic facies but is facilitated by the presence of the continuous grainstone unit that drapes the thrombolite-stromatolite buildups. Thrombolite-stromatolite reefs are composed of individual columns separated by intercolumn fills (Figure 4C, D). Therefore, vertical permeability might be better than horizontal permeability. This might positively influence the continuity and connectivity of unit 2. The complexity of the situation, of course, depends on the type of hydrocarbon being drained: gas insures that any connection allows the drainage of the reservoir. However, when dealing with oil, bypass of oil might occur by having the high-permeability grainstones at the top. Second, if contemplating secondary recovery (e.g., water flooding or gas injection), the mobility ratio of the two phases determines if the displacing phase might channel through the high-permeability zones.

The 3-D outcrop model that was constructed and presented in this article can easily be transferred into reservoir simulators. Future work could involve flow simulations testing the threshold with which the isolated dome-shaped buildups are connected by the grainstone. When the porosity and permeability contrasts between thrombolite-stromatolite reef and grainstone facies are too high, no flow will be present between these different facies, i.e., high permeability and porosity of grainstone facies might cause hydrocarbons to stay behind in the buildups when drained.

CONCLUSIONS

Digital acquisition systems such as differential GPS surveying allowed systematic mapping of a terminal Proterozoic carbonate ramp of the Nama Group, central Namibia. Large amounts of high-resolution data were obtained on the stratigraphic architecture and the geometry and dimensions of thrombolite-stromatolite buildups that developed in the carbonate ramp system. The acquired digital data set of surveyed data points, mapped at meter scale, was integrated with the DEM

and aerial orthophotographs. Both deterministic and stochastic modeling techniques were used to construct 3-D outcrop models. The accuracy with which dimensions of reefal buildups could be computed proved important to model statistically dome-shaped buildups. Calculations and corrections were applied directly to the digital data set and served as input during model building. The final high-resolution 3-D outcrop model depicts the stratigraphic framework of the carbonate ramp including the reefal buildups.

The position of the buildups in the stratigraphic framework provides a good example of favorable conditions for buildup growth during increasing accommodation or low sediment input. Decreasing accommodation and increasing sedimentation rates influence buildup morphology to change from dome shaped to tabular. Key subsurface reservoir parameters such as volumetrics and reservoir continuity and connectivity are directly related to the geometric diversity and facies association of the carbonate buildups.

REFERENCES CITED

- Adams, E. W., S. Schröder, J. P. Grotzinger, and D. S. McCormick, 2004, Digital reconstruction and stratigraphic evolution of a microbial-dominated, isolated carbonate platform (terminal Proterozoic, Nama Group, Namibia): *Journal of Sedimentary Research*, v. 74, p. 479–497.
- Amthor, J. E., J. P. Grotzinger, S. Schröder, S. A. Bowring, J. Ramezani, M. W. Martin, and A. Matter, 2003, Extinction of *Cloudina* and *Namacalathus* at the Precambrian–Cambrian boundary in Oman: *Geology*, v. 31, p. 431–434.
- Banerjee, S., and S. Mitra, 2004, Remote surface mapping using orthophotos and geologic maps draped over digital elevation models: Application to the Sheep Mountain anticline, Wyoming: *AAPG Bulletin*, v. 88, p. 1227–1237.
- Bellian, J. A., C. Kerans, and D. C. Jennette, 2005, Digital outcrop models: Application of terrestrial scanning lidar technology in stratigraphic modeling: *Journal of Sedimentary Research*, v. 75, p. 166–176.
- Blendinger, W., P. Brack, A. Kristoffer Norborg, and E. Wulff-Pedersen, 2004, Three-dimensional modelling of an isolated carbonate buildup (Triassic, Dolomites, Italy): *Sedimentology*, v. 51, p. 297–314.
- Burchette, T. P., and V. P. Wright, 1992, Carbonate ramp depositional systems: *Sedimentary Geology*, v. 79, p. 3–57.
- Dorobek, S. L., and S. L. Bachtel, 2001, Supply of allochthonous sediment and its effects on development of carbonate mud mounds, Mississippian Lake Valley Formation, Sacramento Mountains, south-central New Mexico, U.S.A.: *Journal of Sedimentary Research*, v. 71, p. 1003–1016.
- Dreyer, T., L.-M. Fält, T. Høy, R. Knarud, R. Steel, and J.-L. Cuevas, 1993, Sedimentary architecture of field analogues for reservoir information (SAFARI); a case study of the fluvial Escanilla Formation, Spanish Pyrenees, in S. S. Flint and I. D. Bryant, eds., *The geological modelling of hydrocarbon reservoirs and outcrop analogues*: International Association of Sedimentologists Special Publication 15, p. 57–80.
- Geehan, G., and J. Underwood, 1993, The use of length distributions in geological modeling, in S. S. Flint and I. D. Bryant, eds., *The geological modelling of hydrocarbon reservoirs and outcrop analogues*: International Association of Sedimentologists Special Publication 15, p. 205–212.
- Germes, G. J. B., 1974, The Nama Group in South West Africa and its relationship to the Pan African geosyncline: *Journal of Geology*, v. 82, p. 301–317.
- Germes, G. J. B., 1983, Implications of a sedimentary facies and depositional environmental analysis of the Nama Group in South West Africa/Namibia, in R. M. Miller, ed., *Evolution of the Damara orogen*: Geological Society of South Africa Special Publication 11, p. 89–114.
- Germes, G. J. B., 1995, The Neoproterozoic of southwestern Africa, with emphasis on platform stratigraphy and paleontology: *Precambrian Research*, v. 73, p. 137–151.
- Gresse, P. G., and G. J. B. Germes, 1993, The Nama foreland basin: Sedimentation, major unconformity bounded sequences and multisided active margin advance: *Precambrian Research*, v. 63, p. 247–272.
- Grötsch, J., and C. Mercadier, 1999, Integrated 3-D reservoir modeling based on 3-D seismic; the Tertiary Malampaya and Camago buildups, offshore Palawan, Philippines: *AAPG Bulletin*, v. 83, p. 1703–1728.
- Grötsch, J., O. Suwaina, G. Ajlani, A. Taher, R. El-Khassawneh, S. Lokier, G. Coy, E. van der Weerd, S. Masalmeh, and J. van Dorp, 2003, The Arab Formation in central Abu Dhabi: 3-D reservoir architecture and dynamic modeling: *GeoArabia*, v. 8, p. 47–86.
- Grotzinger, J. P., 2000, Facies and paleoenvironmental setting of thrombolite-stromatolite reefs, terminal Proterozoic Nama Group (ca. 550–543 Ma), central and southern Namibia: *Communications of the Geological Survey of Namibia*, v. 12, p. 221–233.
- Grotzinger, J. P., 2002, Stratigraphy, facies, and paleoenvironmental setting of a terminal Proterozoic carbonate ramp, Nama Group (ca. 550–543 Ma), Namibia: *Johannesburg, South Africa, 16th International Sedimentological Congress, Field Guide*, 71 p.
- Grotzinger, J. P., and J. E. Amthor, 2002, Facies and reservoir architecture of isolated microbial carbonate platforms, terminal Proterozoic–Early Cambrian Ara Group, south Oman salt basin (abs.): *AAPG Annual Meeting Program*, v. 11, p. A67.
- Grotzinger, J. P., S. A. Bowring, B. Z. Saylor, and A. J. Kaufman, 1995, Biostratigraphic and geochronologic constraints on early animal evolution: *Science*, v. 270, p. 598–604.
- Grotzinger, J. P., W. A. Watters, and A. H. Knoll, 2000, Calcified metazoans in thrombolite-stromatolite reefs of the terminal Proterozoic Nama Group, Namibia: *Paleobiology*, v. 26, p. 334–359.
- Hurn, J., 1993, *Differential GPS explained*: Sunnyvale, California, Trimble Navigation Limited, 55 p.
- James, N. P., and P.-A. Bourque, 1992, Reefs and mounds, in R. G. Walker and N. P. James, eds., *Facies models*: Geological Association of Canada, p. 323–347.
- Kennard, J. M., and N. P. James, 1986, Thrombolites and stromatolites: Two distinct types of microbial structures: *Palaios*, v. 1, p. 492–503.
- Kerans, C., and S. W. Tinker, 1997, Sequence stratigraphy and characterization of carbonate reservoirs: *SEPM Short Course Notes* 40, 130 p.
- Kramer, J. H., 1998, Advances in digital field mapping (abs.): *Geological Society of America Annual Meeting Abstracts with Programs*, v. 30, p. 256.

- Krum, G. L., and C. R. Johnson, 1993, A 3-D modelling approach for providing a complex reservoir description for reservoir simulations, *in* S. S. Flint and I. D. Bryant, eds., *The geological modelling of hydrocarbon reservoirs and outcrop analogues: International Association of Sedimentologists Special Publication 15*, p. 253–258.
- Larue, D. K., and H. Legarre, 2004, Flow units, connectivity, and reservoir characterization in a wave-dominated deltaic reservoir: Meren reservoir, Nigeria: *AAPG Bulletin*, v. 88, p. 303–324.
- Li, H., and C. D. White, 2003, Geostatistical models for shales in distributary channel point bars (Ferron Sandstone, Utah): From ground-penetrating radar data to three-dimensional flow modeling: *AAPG Bulletin*, v. 87, p. 1851–1868.
- Lillesand, T. M., and R. W. Kiefer, 2000, *Remote sensing and image interpretation*, 4th ed.: New York, John Wiley & Sons, 724 p.
- Lucia, F. J., 1999, *Carbonate reservoir characterization*: Berlin, Springer-Verlag, 226 p.
- Mancini, E. A., J. C. Llinás, W. C. Parcell, M. Aurell, B. Bádenas, R. R. Leinfelder, and D. J. Benson, 2004, Upper Jurassic thrombolite reservoir play, northeastern Gulf of Mexico: *AAPG Bulletin*, v. 88, p. 1573–1602.
- Mattes, B. W., and S. Conway Morris, 1990, Carbonate/evaporite deposition in the late Precambrian–Early Cambrian Ara Formation of southern Oman, *in* A. H. F. Robertson, M. P. Searle, and A. C. Ries, eds., *The geology and tectonics of the Oman region: Geological Society (London) Special Publication 49*, p. 617–636.
- Miller, R. M., 1983, The Pan-African Damara orogen of South West Africa/Namibia, *in* R. M. Miller, ed., *Evolution of the Damara orogen: Geological Society of South Africa Special Publication 11*, p. 431–515.
- Murillo-Muneton, G., and S. L. Dorobek, 2003, Controls on the evolution of carbonate mud mounds in the Lower Cretaceous Cupido Formation, northeastern Mexico: *Journal of Sedimentary Research*, v. 73, p. 869–886.
- Peters, J. M., J. Filbrandt, J. P. Grotzinger, M. Newall, M. Shuster, and H. A. Al-Siyabi, 2003, Surface-piercing salt domes of interior north Oman, and their significance for the Ara carbonate 'stringer' hydrocarbon play: *GeoArabia*, v. 8, p. 1–40.
- Pratt, B. R., 2002, Storms versus tsunamis: Dynamic interplay of sedimentary, diagenetic, and tectonic processes in the Cambrian of Montana: *Geology*, v. 30, p. 423–426.
- Saylor, B. Z., J. P. Grotzinger, and G. J. B. Germs, 1995, Sequence stratigraphy and sedimentology of the Neoproterozoic Kuibis and Schwarzrand Subgroups (Nama Group), southwestern Namibia: *Precambrian Research*, v. 73, p. 153–171.
- Saylor, B. Z., A. J. Kaufman, J. P. Grotzinger, and F. Urban, 1998, A composite reference section for terminal Proterozoic strata of southern Namibia: *Journal of Sedimentary Research*, v. 68, p. 1223–1235.
- Schröder, S., B. C. Schreiber, J. E. Amthor, and A. Matter, 2003, A depositional model for the terminal Neoproterozoic–Early Cambrian Ara Group evaporites in south Oman: *Sedimentology*, v. 50, p. 879–898.
- Smith, O. A., 1998, Terminal Proterozoic carbonate platform development: Stratigraphy and sedimentology of the Kuibis Subgroup (ca. 550–548 Ma), northern Nama Basin, Namibia: Master's Thesis, Massachusetts Institute of Technology, Cambridge, Massachusetts, 132 p.
- Stanistreet, I. G., P. A. Kukla, and G. Henry, 1991, Sedimentary basin responses to a late Precambrian Wilson cycle: The Damara orogen and Nama foreland, Namibia: *Journal of African Earth Sciences*, v. 13, p. 141–156.
- Thurmond, J. B., J. P. Grotzinger, and W. J. Lyons, 1999, Three-dimensional digital mapping of stratigraphic geometries; issues and examples of practical implementation (abs.): *Geological Society of America Annual Meeting Abstracts with Programs*, v. 31, p. 193.
- Tucker, M. E., F. Calvet, and D. Hunt, 1993, Sequence stratigraphy of carbonate ramps: Systems tracts, models and application to the Muschelkalk carbonate platforms of eastern Spain, *in* H. W. Posamentier, C. P. Summerhayes, B. U. Haq, and G. P. Allen, eds., *Sequence stratigraphy and facies associations: International Association of Sedimentologists Special Publication 18*, p. 397–415.
- Verwer, K., J. A. M. Kenter, B. Maathuis, and G. Della Porta, 2004, Stratal patterns and lithofacies of an intact seismic-scale Carboniferous carbonate platform (Asturias, northwestern Spain): A virtual outcrop model, *in* A. Curtis and R. Wood, eds., *Geological prior information: Informing science and engineering: Geological Society (London) Special Publication 239*, p. 29–41.
- von Neumann, J., 1951, Various techniques used in connection with random digits: *U.S. National Bureau of Standards Applied Mathematics Series*, v. 12, p. 36–38.
- Watters, W. A., and J. P. Grotzinger, 2001, Digital reconstruction of calcified early metazoans, terminal Proterozoic Nama Group, Namibia: *Paleobiology*, v. 27, p. 159–171.
- Weber, K. J., 1986, How heterogeneity affects oil recovery, *in* L. W. Lake and H. B. Carroll, eds., *Reservoir characterization*: Orlando, Florida, Academic Press, p. 487–544.
- White, C. D., and M. D. Barton, 1999, Translating outcrop data to flow models, with applications to the Ferron Sandstone: *Society of Petroleum Engineers, Reservoir Evaluation and Engineering Journal*, v. 2, p. 341–350.
- White, C. D., and B. J. Willis, 2000, A method to estimate length distributions from outcrop data: *Mathematical Geology*, v. 32, p. 389–419.
- Willis, B. J., and C. D. White, 2000, Quantitative outcrop data for flow simulation: *Journal of Sedimentary Research*, v. 70, p. 788–802.
- Wolf, P. R., 2002, Surveying and mapping: History, current status, and future projections: *Journal of Surveying Engineering*, v. 128, p. 79–107.
- Wright, V. P., and T. P. Burchette, 1998, Carbonate ramps: *Geological Society (London) Special Publication 149*, 465 p.